Transcriptional control of *hgcAB* by an ArsR-like regulator in *Pseudodesulfovibrio mercurii* ND132

Caitlin M. Gionfriddo*[1], Ally Bullock Soren[1], Ann Wymore[2], D. Sean Hartnett[1], Mircea Podar[2], Jerry M. Parks[2], Dwayne A. Elias[3], Cynthia C. Gilmour[1]

[1]Smithsonian Environmental Research Center, Edgewater, MD 21037, USA

[2] Biosciences Division, Oak Ridge National Lab, Oak Ridge, TN 37830, USA 11 22

[3]Elias Consulting, LLC, Knoxville TN, USA 37934

*Corresponding author, gionfriddoc@si.edu

RUNNING TITLE: ArsR regulated expression of mercury methylation genes

KEYWORDS: mercury biogeochemistry, arsenic resistance, ArsR, hgcAB, methylmercury

ABSTRACT

The *hgcAB* gene pair encodes mercury (Hg) methylation capability in a diverse group of microorganisms, but its evolution and transcriptional regulation remain unknown. Working from the possibility that the evolutionary function of HgcAB may not be Hg methylation, we test a possible link to arsenic resistance. Using model Hg-methylator *Pseudodesulfovibrio mercurii* ND132, we specifically evaluated transcriptional control of *hgcAB* by a putative ArsR encoded upstream and co-transcribed with *hgcAB*. This regulator shares homology with ArsR repressors of arsenic resistance and S-adenosyl-homocysteine (SAH) responsive regulators of methionine biosynthesis but is distinct from other ArsR/SahR in *Pseudodesulfovibrio mercurii* ND132. Using qPCR and RNA-seq analyses we confirmed this ArsR regulates *hgcAB* transcription, and is responsive to arsenic and SAH. Additionally, RNA-seq indicated a possible link between *hgcAB* activity and arsenic transformations by *Pseudodesulfovibrio mercurii* ND132, with significant up-regulation of other ArsR-regulated arsenic resistance operons alongside *hgcAB*. Interestingly, wild-type ND132 was less sensitive to AsV (but not AsIII) than an *hgcAB* knockout strain, supporting the idea that *hgcAB* may be linked to arsenic resistance. Arsenic significantly impacted Hg-methylation rates by ND132, however, responses varied with culture conditions. Differences in growth and overall metabolic activity did not account for arsenic impacts on methylation. One goal of this research is to better predict MeHg production in nature. However, we found that *hgcAB* gene and transcript abundance was not a good predictor of Hg-methylation rates. Our finding that *hgcAB* activity is linked to arsenic may hold clues to the possible environmental drivers of horizontal transfer of *hgcAB*.

41 **IMPORTANCE**

42 This work reveals a link between microbial mercury methylation and arsenic resistance and may
43 hold clues to the evolution of mercury methylation genes (*hgcAB*). Microbes with *hgcAB*
44 produce methylmercury, a strong neurotoxin that readily accumulates in the food web. This
45 study addresses a critical gap in our understanding about the environmental factors that control
46 *hgcAB* expression. We show that *hgcAB* expression is controlled by an ArsR-like regulator
47 responsive to both arsenic and S-adenosyl-homocysteine in our model organism,
48 *Pseudodesulfovibrio mercurii* ND132. Exposure to arsenic also significantly impacted
49 *Pseudodesulfovibrio mercurii* ND132 mercury methylation rates. However, expression of *hgcAB*
50 was not always a good predictor of Hg methylation rates, highlighting the roles of Hg
51 bioavailability and other biochemical mechanisms in methylmercury production. This study
52 improves our understanding of the controls on *hgcAB* expression which is needed to better
53 predict environmental methylmercury production.

54

55 **INTRODUCTION**

56 Microorganisms play a major role in controlling the form and fate of mercury (Hg) in aquatic
57 environments. Methylmercury (MeHg), an organic Hg compound, is a neurotoxin that
58 accumulates in food sources and is primarily produced by microorganisms(1). The *hgcAB* gene
59 pair that encodes Hg methylation capability(2) is widespread in anaerobic environments and
60 present in genomes spanning a diverse group of metabolic clades(3-5). Hg methylation capability
61 is a species-specific trait that is often associated with low abundant taxa in the microbiome(3, 6).
62 Currently, we do not have a good metric for estimating the prevalence of the mercury
63 methylation trait among microbiota. However, in environmental metagenomic studies of mercury

64 methylator environments, sequencing coverage of *hgcAB* genes is often low compared to other
65 functional genes(7). For example, the coverage of dissimilatory sulfite reductase genes (*dsr*) in
66 metagenomic assemblies is often 3-34x higher than *hgcAB*(7). Despite the association of sulfate-
67 reducing bacteria (SRB) with Hg methylation, the *hgcAB* gene pair is found in only ~12% of
68 publicly sequenced SRB in the Deltaproteobacteria (although *hgcAB* is more common within
69 some genera including *Pseudodesulfovibrio*)(8-10). Of the roughly 3,078 sequenced
70 Deltaproteobacteria genomes in the NCBI reference database, only 368 were identified as
71 potential Hg-methylators when the Hg-MATE database was compiled(7, 11). Within other phyla,
72 especially environmental metagenome assembled genomes from the *Bacteroidetes*, *Nitrospirae*,
73 PVC superphylum and candidate phyla radiation, *hgcAB* distribution further diverges from
74 species trees but follows environmental patterns and suggests horizontal gene transfer of this
75 capability(4, 6). Not all Hg-methylators share the same methylation capabilities, indicating that
76 Hg uptake, Hg(II) binding to HgcAB, *hgcAB* transcription, enzyme regulation, or protein
77 structure may control Hg methylation capacity and efficiency(12-17). Currently, we have a
78 limited understanding of the biochemical constraints on Hg-methylation and the environmental
79 conditions that resulted in the conservation of *hgcAB* in Bacterial and Archaeal genomes.
80 Despite the identification of two genes that encode Hg methylation capability, the
81 mechanism by which methylation is performed within the cell is largely speculative. The genes
82 encode a corrinoid (i.e., vitamin B_{12}-dependent) protein (HgcA), and a 2[4Fe-4S] ferredoxin
83 (HgcB), that could be used as a methyl carrier and electron donor in corrinoid cofactor reduction,
84 respectively (2, 18). Both genes (*hgcA* and *hgcB*) are required for Hg methylation (2, 19).
85 Corrinoid-dependent methyltransferases are utilized in a range of microbial metabolic pathways
86 in the methylation of amino acids, proteins, DNA, and other intermediates(20, 21). In anaerobic

87 microorganisms, corrinoid-dependent enzymes drive methionine and acetyl-CoA production (22,
88 23). Both pathways have been linked to Hg methylation, and the methyl transfer to Hg is thought
89 to occur via a similar mechanism (18, 24-27). HgcA consists of a cytoplasmic corrinoid binding
90 domain and a transmembrane domain. The cytoplasmic domain of HgcA shares homology with
91 the C-terminal domain of the large subunit of the corrinoid iron-sulfur protein (CFeSP) utilized
92 in methyl transfer in the Wood-Ljungdahl (i.e., reductive acetyl-CoA) pathway (2, 18).
93 Further, the native function(s) of HgcA and HgcB remaining unknown. Although HgcAB
94 function has been linked to one-carbon metabolism(28), we don't know if these proteins carry
95 out any functions independent of Hg methylation. Redox transformations of metals and
96 metalloids are often part of detoxification mechanisms or energy production. However,
97 biomethylation of Hg does not provide any observed benefit to the cell, and Hg methylation
98 capability is not induced by Hg(II)(28-30). Deletion of the *hgcAB* gene pair does not appear to
99 hinder cell growth or produce any major phenotype in *Pseudodesulfovibrio mercurii* ND132 (2,
100 28). While some photosynthetic bacteria have been shown to use Hg(II) as an electron acceptor
101 during photosynthetic and fermentative growth(31), Hg-methylating organisms are not able to
102 use Hg species as growth substrates(30). Resolving the native biochemical function of HgcAB is
103 needed to identify the metabolic conditions that mediate HgcAB activity and function.
104 Understanding the biological and geochemical factors that influence MeHg production is
105 necessary for predicting the impacts of contamination and remediation efforts on natural
106 systems.
107 Building predictive models for net MeHg production in aquatic environments is a
108 challenge(32). There are several microbial, physical, and geochemical parameters that influence
109 mercury biogeochemistry in aquatic environments, including but not limited to Hg complexation,

110 availability of terminal electron acceptors, shifts in redox, the composition or availability of
111 organic matter, and the presence, abundance, and activity of Hg-cycling microorganisms(1, 33,
112 34). While the *hgcAB* gene pair can be used to identify potential Hg-methylators in a
113 microbiome(6), to date, *hgcAB* gene abundance alone has rarely provided a useful indicator of
114 environmental MeHg production(35-38). Measuring metabolic and *hgcAB* activity of Hg-
115 methylators has been proposed to improve predictions(36, 39-42). However, it is unclear whether
116 we can relate *hgcA* activity to Hg methylation rates(29). There are several significant unknowns,
117 including whether *hgcAB* is transcriptionally regulated, what geochemical conditions influence
118 *hgcAB* transcription, and if higher expression of *hgcAB* transcripts increases MeHg production.
119 Previous work indicates that *hgcAB* transcription is not regulated by Hg(28-30). A possible
120 overlap with microbial mechanisms for arsenic resistance has been proposed, as several studies
121 have shown that *hgcAB* is co-localized with genes that encode for arsenic resistance in some Hg-
122 methylators(4, 8, 43), including an ArsR-like regulator. In Hg-methylating members of the
123 *Pseudodesulfovibrio*, this *arsR*-like gene is often found with *hgcAB*, and has been shown to be
124 co-transcribed with *hgcAB*(8).
125 In this study, we test the ability of the ArsR-like regulator co-transcribed with *hgcAB* to
126 enhance both *hgcA* transcription and Hg methylation itself in *Pseudodesulfovibrio mercurii*
127 ND132, a model Hg methylator(9, 30). Two transcriptional responses were tested, one to arsenic
128 using arsenite (As(III)) and arsenate (As(V)), and the second to S-adenosyl-homocysteine (SAH)
129 using methionine and adenosine-2',3'-dialdehyde. We chose these test conditions due to the
130 shared homology between this potential *hgcAB* regulator and helix-turn-helix regulons in other
131 sulfate-reducing bacteria that are responsive to As(III) (ArsR) and S-adenosyl-homocysteine
132 (SahR). These regulate arsenic resistance or methionine biosynthesis, respectively, a(44-46).

133 There are possible biochemical overlaps between Hg-methylation and S-adenosyl-methionine
134 (SAM)- mediated methylation(47, 48) , including those utilized in methyl-arsenic or methionine
135 biosynthesis. Experiments were designed to test whether *hgcAB* transcription is regulated by
136 ArsR/SahR.

137 In addition to evaluating potential *hgcA* regulators, another goal of this study was to test
138 the idea that Hg-methylation rates are related to *hgcAB* expression rates. We hypothesized that
139 geochemical culture conditions that increase *hgcAB* expression in *Pseudodesulfovibrio mercurii*
140 ND132 will lead to higher Hg methylation rates than analogous conditions. Outcomes of this
141 study have important implications for modelling Hg-methylation potential in the environment.
142

143 **METHODS**

144

145 **Bacterial strains and culture media:** For this study, we used the sulfate-reducing Hg-
146 methylator and incomplete-oxidizer *Pseudodesulfovibrio mercurii* ND132 (previously
147 *Desulfovibrio desulfuricans* ND132) as a model organism for understanding the mechanism and
148 genetic regulation of Hg methylation(9, 30). *P. mercurii* ND132 has a well annotated genome,
149 can grow on a number of substrates including lactate/sulfate, pyruvate/fumarate,
150 formate/acetate/sulfate, and formate/acetate/fumarate(49). Furthermore, knock-out strains
151 (Δ*hgcA,B*) of *P. mercurii* ND132 have been used to show the requirement of *hgcA* and *hgcB* for
152 Hg methylation(2, 19). For this study, we used *P. mercurii* ND132 wild-type and mutant glycerol
153 stock cultures from Dr. Dwayne Elias' culture collection. Since these experiments began, wild-
154 type *Pseudodesulfovibrio mercurii* ND132 has been deposited into DSMZ (type strain DSM
155 110689) and ATCC (ATCC TSD-224) culture collections. The Hg-methylation knock-out strain

156 (Δ*hgcAB*) of *P. mercurii* ND132 was originally sourced from Judy Wall(2). Stock cultures were
157 stored at -80ºC in lactate-sulfate media and 10% v/v glycerol.
158 ND132 is capable of fumarate respiration using pyruvate as an electron donor(9). For
159 most assays, *P. mercurii* ND132 was grown in this way on either CCM(50) or Estuarine
160 Pyruvate Fumarate (EPF) medium(9). Both media contain 40 mM pyruvate and 40 mM
161 fumarate. CCM is a defined medium, while EPF includes 0.5% yeast extract. Both media were
162 buffered to pH 7.2 using MOPS and include vitamin and mineral additions. Media were reduced
163 with 0.1 mM (CCM) or 0.05 mM (EPF) cysteine-HCl to remove trace oxygen contamination.
164 Other amendments varied by experiment. All media contained resazurin as a redox indicator. For
165 some arsenic toxicity assays, ND132 was also grown on CCM media with lactate (60 mM) and
166 sulfate (30 mM) as electron donor and acceptor. All culture work was done at 31 ± 1 °C.
167
168 **Experimental assays for testing regulators of Hg methylation and *hgcAB* transcription:** We
169 evaluated the potential transcriptional response of a putative *hgcAB* regulator to S-adenosyl-
170 homocysteine (SAH) and arsenic. We also evaluated potential influence of *hgcA* expression on
171 Hg methylation using batch culture and washed cell approaches. For all assays, cultures were
172 started from freezer stocks. In all cases, cells were grown on CCM or EPF media. Out of the
173 freezer, cells were grown to mid-late exponential phase, then inoculated at 10% v/v into medium
174 containing one of the four test conditions, or unamended control medium. In defined CCM media
175 the test amendments were: 0.2 mM sodium arsenite, 2.0 mM sodium arsenate, 1 mM methionine,
176 0.1 mM adenosine-2'3'-dialdehyde, and 1 nM of HgCl. In EPF media, arsenic concentrations
177 were reduced to 0.02 mM sodium arsenite and 0.2 mM sodium arsenate. Amendment
178 concentrations for expression and methylation studies were chosen based on toxicity tests (see

179 below). Arsenic concentrations selected were the highest levels that allowed unimpacted growth,
180 which was specific to each medium. In qPCR expression experiments conducted over the growth
181 curve, both control and amendment cultures were grown without added Hg. In the washed-cell
182 assays and Hg-methylation assays performed in culture, all treatments including the control were
183 spiked with 1 nM isotopically enriched ^{201}Hg.

184 Methylation assays were carried out in triplicate by the addition of 1 nM isotopically
185 enriched ^{201}Hg (98.1% purity; Oak Ridge National Laboratory) (in 1% v/v HCl). Uninoculated
186 sterile medium with and without treatment amendments served as abiotic controls. Methylation
187 assays ran 100 minutes, after which aliquots of unfiltered culture were immediately acidified
188 (0.5% v/v HCl) and frozen (-20°C) for Me^{201}Hg analysis. Experimental timeframes were selected
189 on the basis of previous kinetic experiments demonstrating a plateau in MeHg production by
190 strain ND132(17).

191 Methylation assays were performed using either washed cells or batch culture cells. For
192 washed cell assays, cells were harvested at mid log phase (OD_{600} ~ 0.2) from batch culture and
193 washed and resuspended in a minimal wash buffer as described previously(51). The salt buffer
194 contained 1 mM pyruvate and 1 mM fumarate, reduced with 0.5 mM cysteine-HCl, and buffered
195 to pH 7.5. For batch culture experiments, culture aliquots from mid log phase (OD_{600} ~ 0.2) were
196 directly spiked with ^{201}Hg. In most cases, the concentration of filterable and total ^{201}Hg was
197 measured immediately after the ^{201}Hg spike, and at the end of the methylation assays (and in
198 some cases through time during the assays). Samples were filtered through 13mm diameter 0.22
199 μm CellTreat® MCE membrane syringe filters. For most studies we also measured pH, optical
200 density at 600 nm wavelength (OD_{600}), acridine orange direct cell counts (AODC), and sulfide
201 concentration over the course of the assay. Additionally, for some studies we measured short-

202 chain fatty acids and/or CO_2 production as indicators of cellular activity. All culture
203 manipulations were carried out in a Coy® glove bag under an O_2-free atmosphere.
204 Culture aliquots were saved for RNA extraction before the assays and from each assay
205 replicate at the end of the time-course (t = 100 minutes). For RNA extraction, cells were
206 harvested from batch cultures and methylation assays at 2,800 x g for 10 minutes. The cell pellet
207 was resuspended in 1 mL TRIzol™ Reagent (Invitrogen), and kept at -20°C prior to nucleic acid
208 extraction.

209 **Hg and MeHg analyses:** Isotope-specific total Hg and MeHg concentrations were measured
210 using modifications of EPA Methods 1631 (EPA-821-R-01-023, Mar 2001) and 1630 (EPA-821-
211 R-01-020, Jan 2001) respectively, with inductively coupled plasma mass spectrometry (ICP-MS)
212 detection. Details of the analytical method and QA/QC (Table S1) are provided in the SI.

213 **Other analytical methods:** Sulfide was analyzed using a sulfide selective electrode with an
214 Ag−AgCl reference electrode (Thermo Scientific) and was calibrated against Pb-titrated Na_2S
215 standards made in sulfide antioxidant buffer (SAOB). Saturated Na_2S stocks were made from
216 washed crystals in degassed ultra-pure water and held in N_2-filled sealed serum vials until use.
217 SAOB contains 2 M NaOH, 0.2 M EDTA and 0.2 M ascorbic acid, in degassed ultra-pure water
218 and sealed under N_2 until use. Organic acids (acetate, pyruvate, fumarate, and succinate) (0.5–
219 200 μM) were determined with a Dionex™ Integrion HPIC equipped with an AS11-HC column
220 at 35 ºC with a KOH gradient of 1–60 mM with an ICS-5000$^+$ EG effluent generator system
221 (Thermo Fisher Scientific). Sample volumes of 10 μl were injected with a Dionex™ AS-AP
222 auto-sampler at room temperature.

223 Cell counts were done manually using acridine orange staining. Cells were fixed at a
224 dilution of 1:100, with 0.1 mL of cell culture preserved in 9.1 mL of 20 mM phosphate buffer
225 solution (PBS) and 0.8 mL glutaraldehyde, and stored in the fridge prior to slide prep. Slides
226 were made by combining 0.2 mL of 0.1% acridine orange and 1.9 mL of fixed cells in
227 microcentrifuge tubes and allowing 1 hr at room temperature in the dark for staining. The stained
228 cells were mixed with 1 mL of 20 mM PBS and collected on filters via vacuum. Counts were
229 performed manually and averaged from 10 different grids over a 0.01 mm^2 area.
230 CO_2 production was measured over time in the headspace of serum vials containing
231 culture aliquots, after purging headspace w/ O_2-free N_2 for ~5 min. All measurements were made
232 from duplicate aliquots for each treatment. The 100 ml serum vials contained either 5 ml of
233 culture, or 25 mL of washed cells in salt buffer. Headspace CO_2 was measured hourly after an
234 initial equilibration period using a LICOR LI-7000 CO_2 analyzer. Total inorganic carbon
235 production was calculated from headspace CO_2 concentrations based on temperature, pH, the
236 Henry's Law constant for CO_2 and equilibrium among dissolved inorganic carbon (DIC) species.
237 DIC production rates were calculated from the linear portion of the slope with time
238
239 **RNA extraction:** Cell cultures were pelleted at 2,800x g for 10 minutes, excess media removed,
240 and then resuspended in 1 mL of TRIzol™ reagent (Invitrogen), and stored at -20 ºC until
241 processing. RNA was extracted following TRIzol protocol, which involves a phenol-chloroform
242 extraction, isopropanol precipitation, and ethanol cleaning step. Extracted RNA was further
243 purified using RNeasy Clean-up kit (Qiagen), and DNAse treatment with TURBO DNA-free™
244 Kit (Thermo Fisher). RNA concentration was measured using a Qubit™ RNA HS assay kit on
245 the Qubit 3.0 Fluorometer (Thermo Fisher), and purity was determined by NanoDrop (Thermo

246 Fisher). gDNA contamination was assessed by performing a qPCR with DNase-treated RNA
247 prior to reverse transcription. cDNA synthesis was performed using iScript™ cDNA Synthesis
248 Kit (Biorad), and cDNA concentration was measured using Qubit™ ssDNA assay kit on the
249 Qubit 3.0 Fluorometer (Thermo Fisher). cDNA was diluted to 1 ng/uL with RNase-free water
250 prior to qPCR.
251
252 **Real-time quantitative PCR (qPCR):** qPCR reactions were set up on a 96-well plate with each
253 standard and biological cDNA sample run in triplicate. Each well contained 1 ng of cDNA, 0.25
254 µM forward and reverse primer, 0.02 µL ROX reference dye (Bio-Rad), 10 µL iQ SYBR Green
255 Supermix (Bio-Rad), and 1xTE Buffer (pH 8), filled to 20 µL total volume. For standard curves,
256 we used serial dilutions of 4.2 ng/µL (measured on Qubit™) gDNA extracted from pure culture
257 *P. mercurii* ND132 wild type, estimated to be equivalent to 10^6 copies/µL based on the size of
258 the genome (3.8 Mbp)(49). All standards and samples of each primer set were amplified on the
259 same plate, with each plate only containing one target or reference gene. All qPCR analyses from
260 the same experiment were performed in succession with the same standard curve. Custom-
261 designed oligo primers were used to amplify 107 nt bp target region of *hgcA* (DND132_1056-
262 hgcA-F, DND132_1056-hgcA-R) and 180 nt bp region of the *arsR*-like gene before *hgcA*
263 (DND132_1054-arsR-F, DND132_1054-arsR-R) (Table S2). Three single-copy housekeeping
264 genes that encode recombinase subunit A (*recA*), gyrase subunit A (*gyrA*), and gyrase subunit B
265 (*gyrB*) were used for normalization of expression of genes of interest. These housekeeping genes
266 were chosen for normalization due to their observed expression stability in ND132 wild-type
267 transcriptomes (data not shown). Custom primers were designed to amplify a 153 nt bp region of
268 *recA* (DND132_1603, DND132_1603-recA-F, DND132_1603-recA-R), 148 nt bp region of

269 *gyrA* (ND132_2285, DND132_2285-gyrA-F, DND132_2285-gyrA-R), and 182 nt bp of *gyrB*
270 (DND132_2284, DND132_2284-gyrB-F, DND132_2284-gyrB-R). Primers were designed to
271 function over the same annealing temperature (65 °C), and the same thermocycler protocol was
272 used to amplify each gene: polymerase activation for 3 minutes at 95 °C, followed by 32 cycles
273 of denaturing for 15 seconds at 95 °C, and annealing for 20 seconds at 65 °C, followed by a melt
274 curve of 0.1 °C/s from 65 °C to 95 °C, ending with 15 seconds at 95 °C.
275
276 **RNA-seq transcriptomics:** RNA sequencing was performed on clean, DNase-treated RNA
277 extracted from the batch culture and washed-cell Hg-methylation assays. For the washed-cell
278 assays, only RNA from the control, As(III), and As(V) treatments were sent for RNA-seq. All
279 treatments from the culture Hg methylation assays were sent for sequencing. Three biological
280 replicates for each treatment were sequenced. Library prep and sequencing were performed by
281 Genewiz (Azenta Life Sciences, NJ). Ribosomal RNA (rRNA) depletion was performed during
282 library preparation using three probes from QIAGEN FastSelect rRNA 5S/16S/23S Kit (Qiagen,
283 Hilden, Germany), respectively. RNA sequencing libraries were prepared using NEBNext Ultra
284 II RNA Library Preparation Kit for Illumina by following the manufacturer's recommendations
285 (NEB, Ipswich, MA, USA). Briefly, enriched RNAs are fragmented for 15 minutes at 94 °C,
286 then first and second strand cDNA are synthesized. cDNA fragments are end repaired and
287 adenylated at the 3' ends, and universal adapters are ligated to cDNA fragments, followed by
288 index addition and library enrichment with limited cycle PCR. Sequencing libraries were
289 validated using the Agilent Tapestation 4200 (Agilent Technologies, Palo Alto, CA, USA), and
290 quantified using Qubit 2.0 Fluorometer (ThermoFisher Scientific, Waltham, MA, USA) as well

291 as by quantitative PCR (KAPA Biosystems, Wilmington, MA, USA). Multiplexed and clustered
292 sequencing libraries were sequenced using Illumina Hiseq 2x150 bp paired-end configuration.
293 Raw sequencing files were uploaded to KBase(52). Initial read quality was assessed with
294 FastQC, followed by adapter and quality-based trimming with Trimmomatic(53), alignment to
295 the *Pseudodesulfovibrio mercurii* ND132 reference genome
296 (https://www.ncbi.nlm.nih.gov/assembly/GCF_000189295.2) with HISAT2(54), assembly of
297 transcripts from alignment using StringTie(55). Differential expression analysis was performed
298 with DeSeq2(56) and the results were uploaded to Galaxy web platform(57), and we used the
299 public server at usegalaxy.org to produce figures using the Galaxy R scripts.
300
301 **Arsenic analyses:** Arsenic speciation analyses were done at Brooks Applied Labs (Bothell, WA,
302 USA). Samples were collected from culture bottles, filtered (Whatman® cellulose acetate
303 membrane syringe filters 0.45 μm) into BD Vacutainers®, preserved in EDTA and stored at 4 °C
304 in the dark until analyzed. Arsenic (As) speciation analysis, including arsenite [As(III)], arsenate
305 [As(V)], monomethylarsonic acid [MMAs], dimethylarsinic acid [DMAs], and unknown As
306 species were determined on all samples. Arsenic species were chromatographically separated on
307 an ion exchange column and then quantified using inductively coupled plasma collision reaction
308 cell mass spectrometry (ICP- CRC-MS). The results were not method blank corrected and were
309 evaluated using reporting limits adjusted to account for sample aliquot size.
310
311 **Structural modeling**: Structural models of the putative ArsR-like transcriptional regulator from
312 *P. mercurii* ND132 (DND132_1054, Uniprot ID: F0JBE8) were generated with ColabFold(58).
313 ColabFold is an implementation of AlphaFold2(59) that uses MMSeqs2(60) to generate large

314 multiple sequence alignments by searching the UniRef and MGnify databases(61). Based on its
315 sequence similarity to other transcriptional regulators that are known to function as homodimers,
316 we modelled the homodimeric form of the protein using AlphaFold-multimer(62), which is a
317 version of AlphaFold2 trained specifically to model protein complexes. Models were ranked by
318 their average predicted local distance difference test (pLDDT) and predicted TM-score
319 (pTMscore) and the model with the highest pTMscore score was selected for further analysis.
320
321 **Statistical methods:** Statistical modelling was performed in JMP®, Version 16 (SAS Institute
322 Inc., Cary, NC, 1989–2022) and R statistical software (version 4.2.0)(63). Generalized linear
323 models were used to evaluate differences in Hg methylation rates, inorganic carbon production,
324 organic acid production, and growth rates among treatments. Where appropriate, models
325 included time, treatment and any potential interaction terms. In the absence of significant
326 interactions, differences among treatments were evaluated using pairwise comparison of slopes.
327 For qPCR results, a two-sample z-test was used to determine if the difference in *arsR* and *hgcA*
328 expression was significant between treatments and control. For significance testing, the mean
329 and standard deviation of ΔΔCq values for each target gene and treatment were compared to
330 control.
331
332 **RESULTS AND DISCUSSION**
333
334 **An ArsR-like regulator encoded with HgcAB in *Pseudodesulfovibrio*:** A putative arsenic
335 responsive regulator (ArsR) (Gene ID: DND132_1054, Uniprot: F0JBE8) is encoded directly
336 upstream of Hg-methylation genes *hgcA* (Gene ID: DND132_1056, Uniprot: F0JBF0) and *hgcB*

337 (Gene ID: DND132_1057, Uniprot: F0JBF1) in the genome of *P. mercurii* ND132. Potential
338 ArsR-controlled transcriptional regulation of *hgcAB* has been proposed for Hg-methylating
339 members of the *Pseudodesulfovibrio*(8). This potential *hgcAB* regulator shares homology to the
340 metalloregulator ArsR/SmtB protein family (Pfam PF01022), including a DNA-binding helix-
341 turn-helix (HTH) motif. This family of regulators (Pfam PF01022) are responsive to metal ion
342 stress (e.g., As(III), Zn(II), Cd(II)) and in the absence of coordinating metal(loid)s will repress
343 the expression of operons linked to heavy metal resistance(64). This transcriptional family
344 includes the ArsR repressor of the *ars* operon, which often encodes an arsenate reductase with
345 arsenic permeases and exporters(65). However, protein sequence analysis and predictive
346 structure modelling of the *hgcAB* ArsR-like regulator suggests differences in the metal binding
347 domain that may make it distinct from other ArsR family regulators.

348 There are five ArsR family transcriptional regulators annotated in the genome of
349 *Pseudodesulfovibrio mercurii* ND132 (Figure 1). Based on protein sequence analysis, these five
350 ArsR proteins are different from one another, with less than 33% pairwise identity between them
351 (Table S3). We numbered the *arsR* by order of appearance in the genome of *P. mercurii* ND132,
352 and *arsR2* is located directly upstream of *hgcA* and *hgcB* (Figure 1). While in some Hg-
353 methylating bacteria, *hgcAB* is located in the genome with arsenic resistance (*ars*) genes(4, 43),
354 no other *ars* genes are colocalized with *hgcAB* in ND132. However, three of the other *arsR*
355 (*arsR1*, *arsR3*, and *arsR5*) are present with *ars* genes elsewhere in the genome and likely
356 regulate arsenic resistance. The first set of *ars* genes encode ArsR1 (GeneID: DND132_0890)
357 and the first of two methylarsenite efflux permeases, ArsP (DND132_0889)(66). Another *ars*
358 operon encodes ArsR3 (DND132_1317) with the first of two Acr3 family As(III) permeases
359 (DND132_1318) and arsenate reductase, ArsC (DND 132_1319). *P. mercurii* ND132 has a

360 second Acr3 family As(III) efflux permease that is not part of an *ars* operon (DND132_2196).
361 The third *ars* operon is predicted to encode ArsR5 (DND132_2311), another ArsP
362 (DND132_2312), an organoarsenical resistance protein, ArsE (PFam: PF13192, thioredoxin-like
363 protein) (DND132_2313)(67), and a protein of unknown function with a diguanylate cyclase
364 (DGC) motif (Pfam: PF08859, a domain with four conserved cysteines that likely coordinate Zn)
365 (DND132_2314). ArsR repressors of the *ars* operon are predicted to be transcriptionally
366 regulated by As(III) and part of a detoxification pathway for arsenic. From protein sequence
367 analysis of ND132 ArsR2, it is unclear whether expression of *hgcA* and *hgcB* is part of the ArsR
368 regulon and controlled by arsenic.
369 ArsR/SmtB family regulons may not always be associated with heavy metal resistance or
370 arsenic transformations. In addition to regulating arsenic resistance, ArsR regulators have also
371 been shown to influence many other cellular functions in the presence of As(III), including
372 phosphate acquisition/metabolism, sugar transport, chemotaxis, copper tolerance, and iron
373 homeostasis(68). Regulators in the ArsR/SmtB HTH family may also be responsive to substrates
374 other than heavy metals and metalloids. In sulfate-reducing bacteria, an ArsR-like regulon
375 responsive to intracellular concentrations of S-adenosylhomocysteine (SAH) controls SAM-
376 dependent methyl transfer for methionine biosynthesis(44, 45). These SAH-responsive regulators
377 (SahR) are often encoded with adenosylhomocysteinase (AHCY), which catalyzes the hydrolysis
378 of SAH to homocysteine and adenosine. In *P. mercurii* ND132, *arsR4* likely encodes a SahR
379 (Gene ID: DND132_1481, Uniprot: F0JE80). The predicted SahR is encoded with AHCY (Gene
380 ID: DND132_1480, Uniprot: F0JE79) (Figure 1), and has an ArsR-like HTH motif with a SAM-
381 dependent methyltransferase similar to ArsM. Arsenite methyltransferase (ArsM) catalyzes the
382 transfer of a methyl group to arsenite from S-adenosylmethionine (SAM) to form

383 methylarsenicals, and is part of the ArsR regulon(69). Instead of methylarsenical production,
384 ND132 ArsR4 is predicted to control methionine production and be responsive to SAH. No other
385 homologues of ArsM are encoded in the genome of *P. mercurii* ND132. Like *arsR2* which is co-
386 localized with *hgcAB*, *arsR4* is not part of an *ars* operon in *P. mercurii* ND132.
387
388 **Phylogenetic distribution of the ArsR2 *hgcAB* regulator:** Close homologues of the ArsR2
389 regulator from *Pseudodesulfovibrio mercurii* ND132 are present in other *hgc*+ *Desulfovibrio* and
390 *Pseudodesulfovibrio* genomes (Figure S1). To identify potential ArsR2 homologues, we searched
391 for ArsR family proteins encoded before *hgcAB* in *Desulfovibrio* and *Pseudodesulfovibrio*
392 reference genomes from a previous study(9). We also used the HMM of the HTH motif of ArsR
393 (Pfam: PF01022, HTH_5.hmm) to broaden our search and identify all potential HTH family
394 transcriptional regulators encoded in the reference genomes. We used protein sequence
395 alignments and maximum likelihood phylogenies of HMM-hits to identify ArsR2 homologues.
396 Among these genomes, we found ArsR2 homologues only in *hgc*+ *Desulfovibrionaceae*
397 genomes, and always directly upstream of *hgcAB* (Figure S1). Other researchers working with a
398 close relative to ND132, *Pseudodesulfovibrio hydrargi* BerOc1 demonstrated that these *arsR*-
399 like genes and *hgcA* are co-expressed(8). Notably, all but one of the available
400 *Pseudodesulfovibrio* genomes encode the ArsR2 homologue. However, co-occurrence of *arsR*
401 with *hgcAB* does not appear to be phylogenetically conserved in the majority of *hgc*+ genomes
402 of close relatives of *Desulfovibrionaceae* (Figure S1).
403 ArsR family regulators are also encoded with *hgcAB* in genomes from outside of the
404 *Desulfovibrionaceae* family. In *hgc*+ genomes from the Hg-MATE-Db(7, 11), we identified
405 putative ArsR/SmtB family regulators of *hgcAB* in isolate and environmental metagenome-

406 assembled genomes (MAGs) from Deltaproteobacteria, Nitrospira, Spirochaetes,
407 Ignavibacteriae(70) and Bacteroidetes(71), including *Paludibacter jiangxiensis* NM7(72) (Table
408 S4). Based on protein sequence alignments, not all of these putative *hgcAB* regulators are close
409 homologues of the ArsR2 protein from *Pseudodesulfovibrio mercurii* ND132. In some of these
410 genomes, *hgcA* and *hgcB* are also colocalized with other *ars* genes (e.g. *arsC*, *arsB*, *arsM*). It is
411 noteworthy that many of the *hgc*+ MAGs(73) of sediment and groundwater-associated bacteria
412 from the Rifle IFRC site(74) have an ArsR-like regulator encoded with *hgcAB* and *ars* genes.
413 This co-occurrence of *hgcAB* with *ars* genes in MAGs from arsenic-impacted environments has
414 been noted previously(4, 43). For this study, we focused our analytical efforts on understanding
415 possible ArsR-regulated transcription of *hgcAB* in *Pseudodesulfovibrio mercurii* ND132.
416 However, more analysis is needed to explore a possible evolutionary relationship between the
417 *ars* operon and Hg-methylation genes, and whether horizontal gene transfer of *hgcAB* may have
418 been influenced by arsenic.
419
420 **Structural model:** The ArsR2 homologues from *Pseudodesulfovibrio* and *Desulfovibrio* are
421 phylogenetically distinct from other ArsR/SmtB family transcriptional regulators (Figure S2).
422 The protein sequence alignment shows that ArsR2 has some of the conserved invariant residues
423 associated with the HTH family of regulators (Figure S2)(75). To provide additional insight into
424 the structure of the putative *hgcAB* transcriptional regulator (ArsR2, DND132_1054), we
425 generated a homodimeric model of the protein using AlphaFold2(58, 59) (Figure 2). The
426 cysteine-rich site associated with metal(loid) binding is different in ArsR2 compared to ArsR
427 repressors of the *ars* operon. In *E. coli* ArsR (Uniprot: P15905), the As(III) binding site is
428 associated with the three cysteines on the α3 helix (Cys32, Cys34, and Cys37)(64). The

429 cysteines in ND132 ArsR2 (Uniprot: F0JBE8) occur on a coil after helix 2 and a beta strand
430 before helix 4 (Figure S3). The ArsR2 from ND132 includes a cysteine (Cys26) near the N-
431 terminus and four cysteines, Cys47, Cys49, Cys86, and Cys88 (Figure 2 and Figure S3) in each
432 predicted metal(loid) binding site(75). Homologs from several other closely related bacteria of
433 the *Pseudodesulfovibrio* and *Desulfovibrio* have similar structures and cysteine positions (Figure
434 S4), suggesting that some of them may have similar functions. The four-cysteine motif in the
435 metal(loid) binding site is conserved in all ArsR2 homologs found in *Pseudodesulfovibrio* and
436 *Desulfovibrio* genomes (Figure S4) except for *Desulfovibrio brasiliensis* (WP_157054761.1),
437 which has a three-cysteine motif.
438 The metal(loid) binding domain of the putative ArsR of *hgcAB* in *Pseudodesulfovibrio*
439 *mercurii* ND132 (ArsR2, DND132_1054) differs from other ArsR repressors, containing four
440 rather than three cysteines. Arsenite ($As(OH)_3$) is predicted to coordinate with the three cysteine
441 residues of ArsR as As(III), after the loss of its hydroxide ligands(75). However, only two of the
442 three cysteines (Cys32, Cys34) are needed to bind arsenic to ArsR of *Escherichia coli* plasmid
443 R773(76). The presence of four cysteine residues in the metal(loid) binding sites of the ArsR2
444 regulator suggests it may preferentially bind metal(loid) cations such as Zn(II), Cd(II), and Pb(II)
445 like the four-cysteine residues in the binding motif of CadC(75). Alternatively, there could be 3-
446 coordinate binding of As(III) to three of the four cysteine residues as has been proposed with
447 As(III) and the SAM methyltransferase, ArsM(77).
448
449 **Arsenic tolerance in ND132:** The presence of a putative ArsR regulator upstream of *hgcAB*
450 suggests that the ability to methylate Hg may confer As resistance in some microbes. We
451 compared As toxicity between wild-type (WT) ND132 and the *hgcAB* deletion mutant

452 (ND132Δ*hgcAB*) to test the idea that the presence of *hgcAB* in the ND132 genome might
453 contribute to As resistance. We performed growth assays in defined (no yeast extract) CCM-PF
454 and CCM-LS media. Cultures were inoculated into media amended with sodium arsenate (0.2,
455 0.5, 1, 2, 5, or 20 mM) or sodium arsenite (0.02, 0.2, or 0.5 mM) and grown at 30 ºC to
456 stationary phase (Figures 3 and S5).

457 The WT strain was more tolerant of As(V), than the knockout. Specifically, WT ND132
458 growth was unaffected by As(V) levels up to 1 mM on both media, while growth of
459 ND132Δ*hgcAB* was significantly impacted at that level (Figure 3). Results were evaluated
460 statistically by normalizing OD_{600} measurements to matched unamended controls, and then
461 evaluating differences in normalized OD_{600} between the strains. Data from the exponential part
462 of the growth curves were used in the statistical tests. Differences were assessed using general
463 linear models that accounted for As concentration, time, and any significant interactions. The
464 *hgcAB* knockout was significantly more sensitive to As(V) at levels above 0.2 mM on PF
465 medium and at levels above 0.5 mM on LS medium ($p < 0.0001$). Notably there was apparent
466 hormesis in growth of ND132Δ*hgcAB*, with slightly enhanced growth at the lowest tested AsV
467 levels.

468 The WT and knockout strains were equally resistant to As(III), although As(III) toxicity
469 to both was roughly 5-10 times higher than As(V) (Figure S5). Culture chemistry, particularly
470 the formation of As-sulfide complexes, impacted As toxicity. Both wild-type and
471 ND132Δ*hgcAB* cultures had lower tolerance to both As species when grown under sulfidogenic
472 conditions. A yellow mineral precipitate was observed when media with 0.5 mM As(III) was
473 inoculated with sulfidogenic *P. mercurii* ND132 WT and Δ*hgcAB* cultures, and likely was the
474 formation of orpiment (As_2S_3).

475 The reduced As(V) resistance of the *hgcAB* knockout strain suggests that *hgcAB* may
476 confer some As(V) resistance. Or alternatively, the loss the *hgcAB* from the genome may impact
477 other mechanisms of As(V) resistance by ND132. This observation deserves more exploration,
478 especially the lack of differential resistance to the more toxic As(III).
479
480 **ND132 transformation of As(III) and As(V):** *Pseudodesulfovibrio mercurii* ND132 has several
481 ArsR-regulated arsenic resistance operons (Figure 1). These operons are predicted to encode
482 As(V) reductase, As(III) and methylarsenite permeases, and a putative organic arsenic resistance
483 protein. To determine how ND132 may transform arsenic (As), we measured As speciation and
484 mass balance in *P. mercurii* ND132 WT cultures grown with either 0.02 mM sodium arsenite or
485 0.2 mM sodium arsenate in defined CCM-PF media. At these concentrations, As did not affect
486 cell growth rate (Figure S6A). We did not examine whether ND132 gains energy from As(V)
487 reduction.
488 Under these conditions, we found that wild-type *P. mercurii* ND132 reduced As(V) to
489 As(III) and produced potential thioarsenicals from both As(III) and As(V) (Figure S6, Table S5).
490 As concentrations and speciation were measured initially and at the end of exponential growth (7
491 days). ND132 reduced about 25% of added As(V) to As(III) after 7 days, and converted about
492 3% to an unidentified As compound. This compound was tentatively identified as a thioarsenical
493 based on the retention time of the peak (personal communication from Ben Wozniak at Brooks
494 Applied). ND132 converted a higher fraction (roughly 15%) of added As(III) to the presumed
495 thioarsenical compound (Figure S6).
496 In both As(III) and As(V) amended cultures, As speciation at the initial time point
497 matched the spikes, and 70-80% of the added As could be accounted for after 7 days growth.

498 Uninoculated medium served as abiotic controls. There was no significant loss of As or change
499 in As speciation in abiotic controls, including no production of unidentified As compounds. No
500 monomethyl- or dimethylarsenicals were detected in abiotic or cultured samples.
501
502 **Potential transcriptional regulation of *hgcA* by ArsR2:** To help determine the transcriptional
503 controls on the putative ArsR regulator of *hgcAB*, we challenged cells with As and SAH and
504 evaluated expression of both *arsR2* and *hgcA*. We chose these potential regulators because,
505 despite shared homology, the putative *hgcAB* regulator ArsR2 is distinct from other HTH
506 regulators of the ArsR/SmtB family, and its function is unknown. Additionally, since the four
507 other ArsR annotated in the genome of *P. mercurii* ND132 are predicted to regulate either
508 methionine production or As resistance, we speculate that there could be biochemical overlaps
509 between HgcAB function and As resistance or methionine production. We made this inference
510 based on the co-localization of *hgcAB* with other *ars* genes(4, 43), and the shared homology of
511 HgcA/B to corrinoid iron-sulfur proteins utilized in one-carbon metabolism(18, 78), including
512 methionine biosynthesis. Thus, one goal of this work was to test the idea *hgcAB* may be part of
513 the ArsR or SahR regulons. Because of the unusual configuration of the metal(loid) binding
514 motif in ArsR2, we chose to test ND132 response to As(V) as well as As(III) and SAH.
515 We used real-time qPCR to test relative changes in expression of *arsR2* and *hgcA* during
516 growth with potential transcription regulators (e.g., As(III), As(V), SAH). Tests were conducted
517 in defined (i.e., no yeast) CCM media or yeast-enriched EPF media. Expression was normalized
518 to three housekeeping genes and compared to control cultures without added treatments. We also
519 tested for an effect of Hg on *hgcA* transcription and found none (Figure 4). This observation is
520 consistent with previous work that *hgcA* expression and Hg-methylation activity are not induced

521 by Hg(28-30). To evaluate a potential *arsR2* transcriptional response to SAH we tested several
522 compounds in the methionine biosynthesis pathway. Because *P. mercurii* ND132 is not
523 predicted to have an SAH uptake mechanism, we tested for transcriptional response to SAH by
524 growing cells with methionine (1 mM), adenosine-2',3'-dialdehyde (0.1 mM), and equimolar
525 homocysteine with adenosine (0.2/0.2 mM, 0.5/0.5 mM, and 1/1 mM), which enabled the build-
526 up of SAH in the cell. Adenosine-2',3'-dialdehyde is an inhibitor of SAM-dependent
527 methyltransferase. Methionine, homocysteine, and adenosine are metabolites in the SAM cycle,
528 and higher concentrations in culture media should contribute to higher concentrations of SAH
529 compared to cultures grown without these substrates. Growth of *P. mercurii* ND132 was
530 completely inhibited at all concentrations of homocysteine with adenosine. Therefore, this
531 treatment was not used for further expression or Hg methylation experiments.
532
533 **Transcription of *hgcA* is controlled by arsenic and SAH:** We found that ArsR2 regulated
534 *hgcA* expression in *P. mercurii* ND132 and can be responsive to both As and SAH. We observed
535 significantly higher expression (z-test, one-tailed p-value < 0.05; Table S6) of *arsR2* and *hgcA* in
536 *P. mercurii* ND132 cultures compared to control when grown with an SAH-hydrolase blocker
537 (i.e., adenosine-2',3'-dialdehyde) and with As. The transcriptional response varied depending on
538 culture conditions (defined vs. enriched media), and growth phase (i.e., early, mid, or late
539 exponential) (Figure 4). In defined CCM media, we observed significantly higher expression
540 (Table S6) of *arsR2* and *hgcA* in cultures grown with As(V) and As(III) across the growth curve
541 (Figure 3). We only observed significantly higher expression of *arsR2* and *hgcA* from adenosine
542 dialdehyde at late exponential phase (Figure 4). Relative expression of *arsR2* and *hgcA* in
543 enriched media differed from defined media conditions. In enriched media, we observed

544 significantly higher *hgcA* expression in As(V)-amended cultures early in exponential growth, and
545 later in exponential growth for As(III) amended cultures (Table S6). Compared to defined media,
546 we observed significantly higher *hgcA* expression in methionine and adenosine amended cultures
547 at earlier stages of growth (Figure 4). We attribute some of these differences to the presence of
548 additional sulfur-containing metabolites in yeast extract (e.g., methionine) that could have
549 contributed to increased SAH build-up in cultures in enriched media when grown with
550 methionine or adenosine dialdehyde. Without yeast extract, the 1 mM methionine likely did not
551 cause enough SAH build-up to induce a transcriptional response. Unlike in defined media
552 conditions, *arsR2* transcriptional changes did not mirror *hgcA* expression patterns.
553 Differences in *hgcA* expression observed across the growth curve could indicate that the
554 transcriptional response is regulated by an unknown substrate or by an As species produced by *P.*
555 *mercurii* ND132. This effect could vary over the growth curve, as the substrate or products of As
556 metabolism build up in culture or the cell over time. Arsenic speciation analyses showed that *P.*
557 *mercurii* ND132 reduces As(V) to As(III), and produces an unknown thioarsenic species from
558 As(III) (Figure S6). Differences in expression profiles between media could also be attributed to
559 differences in As concentrations, with 10X less As(III) and As(V) used in enriched EPF media
560 than defined CCM media. Reducing the amount of starting As(III) from 0.2 mM to 0.02 mM
561 could have increased the amount of time needed to reach a threshold for transcriptional response.
562 The lower As(III) concentration used in EPF media may explain why increased *arsR2* and *hgcA*
563 expression was only observed in As(III)-amended EPF cultures at late exponential growth
564 (Figure 4). The higher starting concentration of As(V) (0.2 mM) compared to As(III) (0.02 mM)
565 in enriched EPF, may account for the earlier observed transcriptional response in As(V)-

566 amended cultures. Overall, these results show that growing *P. mercurii* ND132 with As(III) or
567 As(V) will significantly increase *hgcA* expression.
568
569 **Metabolites and media components can confound expression analysis:** When cells were
570 washed of culture media and then resuspended in basal salts with treatments, we observed
571 significantly higher *arsR2* and *hgcA* expression due to As but not SAH (Figure 5). Washing cells
572 of media components removed effects of adenosine dialdehyde on *arsR2* and *hgcA* expression
573 observed in culture. Cells that were grown in enriched media with the various treatments were
574 harvested at mid-log (OD_{600} = 0.2; Figure 4B), kept anaerobic, washed of media, and
575 resuspended in a phosphate-salt buffer with the different treatments and 1 nM Hg. This was the
576 same culture in which we measured *arsR2* and *hgcA* expression (Figure 4, EPF mid-log panel).
577 The difference in observed *arsR2* and *hgcA* expression in washed cells (Figure 5C), compared to
578 the culture (before washing) (Figure 4) indicates that build-up of SAH (or another metabolite)
579 during growth with methionine and adenosine dialdehyde likely causes the observed
580 transcriptional response of *arsR2* (DND132_1054). The transcriptional response to As, either as
581 As(III) and or As(V), is more direct and instantaneous. We attribute differences in the
582 transcriptional response to As over the growth curve as resulting from changes in As speciation
583 and toxicity. The qPCR results from washed cells and batch cultures indicate that the *hgcA*
584 regulator (DND132_1054) is responsive to both As and SAH.
585
586 **As affects Hg methylation rates in ND132:** We directly measured the impact of As and SAH
587 on Hg methylation to help confirm that changes in *hgcAB* expression affected Hg methylation
588 rates. Since *hgcA* transcription is regulated by *arsR2* in response to As and SAH, we expected As

589 and SAH should also impact Hg methylation. Arsenic significantly affected *P. mercurii* ND132
590 Hg-methylation rates, but effects varied depending on whether cultures were washed of media
591 components prior to methylation assays. We performed Hg-methylation assays in both cultures
592 and washed cells using mid-log cultures (OD_{600} ~ 0.2, Figure 4B) grown in EPF. Prior to
593 methylation assays, cells were inoculated into media amended with observed expression
594 regulators of *hgcA*: methionine, adenosine dialdehyde, As(III), or As(V). In washed cells
595 harvested at mid-log phase, methionine and As(V)-treated cells produced significantly more
596 MeHg than the control, while As(III) and adenosine significantly reduced MeHg production
597 (Figure 5A). In unwashed cultures, Hg methylation rates were significantly higher in As(III)-
598 amended cultures, but significantly lower in cultures grown with As(V) or adenosine, compared
599 to control (Figure 5B). In batch culture assays, there was no significant difference in MeHg
600 produced in cultures grown with methionine compared to control.
601 Differences in metabolic activity and biomass could account for some of the differences
602 in MeHg production between treatments. When grown with As(V) and methionine, *P. mercurii*
603 ND132 had a steeper growth curve and reached a higher optical density compared to control and
604 other treatments (Figure 4B). In the washed-cell assays, the higher metabolic activity (CO_2
605 respiration rate) (Figure S7) in the methionine treatment could explain some of the higher MeHg
606 production (Figure 5A). In As(V)-treated washed cells, higher MeHg production could not be
607 explained by differences in metabolic activity, biomass, or unfiltered Hg at T_0 (Figure S8, Figure
608 6). Normalization of methylation rates to various measures of cell growth and metabolism did
609 not change the relative impact of treatments (Figure 6). The measured initial concentration of
610 total ^{201}Hg was the same in all bottles, and Hg mass balance was maintained in all bottles (Figure
611 S9). However, the filterable (0.22 μm filters) ^{201}Hg concentration varied among the treatments.

612 Nevertheless, normalization of methylation rates to initial filterable ^{201}Hg concentrations did not
613 alter the relative impact of treatments (Figure 6).
614 In the Hg-methylation assays performed with mid-log cultures, significantly more MeHg
615 was produced in the As(III) treatment (Figure 5B). This effect held true even when normalized to
616 biomass (OD_{600}, cell counts) (Figure S10), pH (Figure S11), metabolic activity (Figure S12), and
617 total Hg (Figure S13) (Figure 5). Hg-methylation rates in As(V)-amended cultures remained
618 significantly lower than control when normalized for these factors (Figure 6). In washed cells
619 and culture media, adenosine-2',3'-dialdehyde appears to limit cell growth and metabolic
620 activity of *P. mercurii* ND132 (Figure 4). MeHg production in adenosine-amended washed cells
621 and batch culture assays were only slightly higher than abiotic controls. It was difficult to
622 decouple the effects of lower metabolic activity and less biomass on limited MeHg production.
623 However, normalizing for biomass (as cell density) put Hg-methylation rates on par with As(V)-
624 amended cultures in media (Figure 6).
625 Differences in Hg bioavailability may contribute to the differences in MeHg production
626 among treatments. Sulfide has strong effects on Hg bioavailability for methylation(12, 30, 79,
627 80) and, although grown without sulfate, ND132 cleaves the S−C bond in cysteine provided in
628 growth medium to release small amounts of sulfide, generally below 10 μM(51). We consistently
629 measured significantly less sulfide in filtered samples from As(V)-amended washed-cell (Figure
630 S7) and batch culture assays (Figure S11) compared to other treatments, including As(III). This
631 observation indicates that As(V) impacts sulfide speciation, possibly by disrupting metabolic
632 pathways that produce reduced sulfide, or precipitation of As species with sulfide. The higher
633 concentrations of As(V) (0.2 mM) could account for the observed differences from As(III) (0.02
634 mM). In addition, the dissolved ^{201}Hg spike is rapidly lost to cell walls and any precipitates in the

635 medium. We observed differences in filterable ^{201}Hg among treatments in both washed cells
636 (Figure S9) and batch cultures (Figure S13). To test the impact of amendments on bioavailable
637 Hg, we normalized methylation rates to the initial concentration of ^{201}Hg in each treatment.
638 Because Me^{201}Hg is exported from cells after production(17), filterable total ^{201}Hg
639 concentrations after T_0 often reflect Me^{201}Hg production (Figure 6).
640
641 **Hg methylation rates decoupled from *hgcA* transcription:** Increased *hgcAB* transcriptional
642 activity did not explain increased MeHg production in most treatments. With the exception of the
643 As(V)-washed cells, we did not observe significantly higher Hg methylation by cells with higher
644 *hgcA* expression compared to control (Figure 5). Despite seeing significantly higher MeHg
645 production by washed cells amended with methionine, and cultures grown with As(III), we did
646 not observe significant differences in *hgcA* expression compared to control in qPCR analyses
647 (Figure 5). Washed cells amended with As(III) had significantly higher *hgcA* expression (Figure
648 5), but produced significantly less MeHg (Figure 6). Similarly, cultures grown with adenosine-
649 2',3'-dialdehyde and As(V) treatments had higher expression of *hgcA*, but produced significantly
650 less MeHg compared to control (Figure 5). This finding was surprising as we expected increased
651 *hgcA* expression to result in higher Hg-methylation rates. However, *hgcA* activity may not have
652 predicted higher Hg-methylation rates because of several factors that we could not account for in
653 this experiment, 1) increased transcription of *hgcAB* may not have resulted in increased
654 translation of HgcAB, 2) Hg availability and uptake by cells may be more rate-limiting than
655 *hgcA*/HgcA activity, 3) Hg complexation with As may interfere with Hg availability for
656 methylation(81), 4) possible competition between As and Hg for binding to HgcAB.
657 Furthermore, the increased Hg methylation rate observed in As(III)-amended cultures could be

658 from increased activity of other unknown proteins essential to the biochemical Hg methylation
659 reaction.
660
661 **As and adenosine increase *hgcA* and *hgcB* expression in ND132 transcriptomes:** RNA-seq
662 analyses of RNA extracted from mid-log washed cells and batch cultures confirm that both *hgcA*
663 and *hgcB* expression is regulated by As and SAH. Growing *P. mercurii* ND132 with As or
664 adenosine dialdehyde appeared to have a significant influence on the transcriptome (Figure S14).
665 We observed significantly higher expression ($|\log FC| > 1.5$, $p < 0.05$) of *arsR2*
666 (DND132_1054), *hgcA* (DND132_1056) and *hgcB* (DND132_1057) in As(III) and As(V)-
667 treated washed cells compared to control (Figure 7). These features were also significantly
668 differentially expressed ($p < 0.05$) in batch cultures amended with As(V) and adenosine
669 dialdehyde (Figure S15). The RNA-seq data show that *hgcB* is being up-regulated with *hgcA*,
670 which is important since both genes are needed for Hg methylation(19). Overall, there were more
671 significant shifts in batch culture transcriptomes compared to washed-cells, with many of the
672 same features being differentially expressed across treatments (Figure S14). Methionine
673 amended batch cultures had the least significant shift in its transcriptome compared to control (n
674 = 4; Figure S16). In *P. mercurii* ND132 cultures grown with adenosine, the predicted SahR
675 regulator encoded by *arsR4* (Gene ID: DND132_1481) was significantly upregulated (log FC =
676 2.36, p = 2.64 E-19) along with the adenosylhomocysteinase-encoding gene *ahcY* (Gene ID:
677 DND132_1480, log FC = 2.31, p = 2.16E-16) (Figure S16). The SAH responsive regulator was
678 not significantly upregulated in any other transcriptome, including methionine-treated cultures.
679 This observation indicates that there may not have been enough build-up of SAH in *P. mercurii*
680 ND132 cultures amended with 1 mM methionine to induce a transcriptional response from SahR

681 or ArsR. There appears to be a cross-reactivity to SAH and As by two ArsR encoded in the
682 genome of *P. mercurii* ND132 *arsR2* (DND132_1054) as well as *arsR5* (DND132_2311)
683 (Figure S15). However, exposure to As(III) or As(V) did not induce a transcriptional response by
684 SahR (*arsR4*, DND132_1481).
685
686 **Co-expression of *hgcAB* with operons of arsenic resistance**: *Pseudodesulfovibrio mercurii*
687 ND132 is resistant to As(V) and As(III), and may also be resistant to organoarsenicals and
688 respire As(V). Both Hg-methylation genes (*hgcA* and *hgcB*) appear to be part of the ArsR
689 regulon and are co-regulated with *ars* operons. Based on RNA sequencing, there were 12 shared
690 features (Figure S14) that had significant differential expression ($|\log FC| > 1.5$, p-value < 0.05)
691 in As-treated washed cells compared to control (Figure 7). These features were also significantly
692 differentially expressed ($p < 0.05$) in batch cultures amended with As(III), As(V), and adenosine
693 dialdehyde (Figure S15). In addition to increased *hgcA* and *hgcB* expression, two ArsR-regulated
694 <u>*ars*</u> operons had significantly higher expression in As-amended washed cells and batch cultures
695 (Figure 7, Figure S15). Operon B (Figure 8) encodes for ArsR3, an Acr3 As(III) efflux
696 permease, and arsenate reductase. Another set of upregulated genes (Operon C) encodes ArsR5
697 and enzymes homologous to those utilized in organoarsenical resistance. Operon C was also
698 upregulated in the transcriptome of adenosine dialdehyde cultures. The other ArsP
699 (DND132_0889) and Acr3 (DND132_2196) permeases encoded outside an operon were not
700 consistently upregulated with the *ars* operons (Figure 7, Figure S15). The only *arsR* gene of *P.*
701 *mercurii* ND132 that was not significantly differentially expressed in any transcriptome was
702 *arsR1* (DND132_0890).
703

704 In As(III) washed cells and As(V) and adenosine batch cultures, an operon with possible
705 links to arsenic or polysulfide respiration was upregulated compared to control. The set of genes
706 (Operon D, Figure 8) encodes possible homologues of the As(V) respiratory reductase (Arr) or
707 polysulfide reductase (Psr) complexes. Since transcription of these genes was increased by
708 As(III), we speculated that their encoded function may relate to As respiration. The genes encode
709 homologues of ArrA (DND132_2597), ArrB (DND132_2598), and ArrC (DND132_2599), and
710 are respectively annotated in *P. mercurii* ND132 as a molybdopterin oxidase, an Fe-S cluster-
711 containing hydrogenase, and formate dehydrogenase gamma subunit protein. The Arr complex is
712 related to the DMSO-molybdopterin (DMSO-MPT) reductase family, with Arr subunit A having
713 a Mo/W-*bis*(pyranopterin guanosine dinucleotide) cofactor in its active site and a [4Fe-4S]
714 center, and Arr subunit B with four [4Fe-4S] clusters(82). A diverse range of microorganisms
715 can respire As(V) for energy using ArrAB(83), including *Chrysiogenes arsenatis*, *Shewanella*
716 strain ANA-3, *Alkaliphilus oremlandii* and *Geobacter* sp. Strain OR-1(84, 85). In some
717 microorganisms, ArrAB can function as a bidirectional enzyme(86), oxidizing As(III) to As(V).
718 Often, ArrAB are encoded in microbial genomes alongside genes of the *ars* operon. However, in
719 *P. mercurii* ND132 the putative operons are not co-localized. The ND132 ArrA homolog
720 includes the conserved molybdenum and Fe-S binding domains found in known functional
721 respiratory As(V) reductases but is missing some of the key active-site residues(86).
722 Instead, operon D (Figure 8) may encode for polysulfide or thiosulfate reduction rather
723 than As(V) respiration. Based on the phylogenetic relationship between the putative ArrA in *P.*
724 *mercurii* ND132 with other DMSO-MPT family proteins, the protein encoded by DND132_2597
725 is more closely related to bacterial polysulfide reductase (PsrA) than ArrA from known As(V)-
726 respiring bacteria (Figure S17). Microbes in deep-sea vents and hydrothermal springs use the

727 membrane protein complex PsrABC to couple periplasmic polysulfide or thiosulfate reduction
728 with quinone oxidation(87). The operon in *P. mercurii* ND132 also encodes homologues of
729 cytochrome *c* oxidase (DND132_2596) and two rhodanese-domain proteins (DND132_2600,
730 DND132_2601), one of which (DND132_2600) is significantly upregulated in As(III) cells. A
731 second cluster of putative *psrAB* genes (DND132_1314, DND132_1313) are present elsewhere
732 in the genome (Figure S17), and likely encode for cytoplasmic sulfur reduction(88). The
733 transcription of these *psrAB* genes was not significantly affected by As or SAH. The DMSO-
734 MPT family of proteins that includes Psr and Arr has been implicated in thioarsenic production.
735 The geothermal isolate *Pyrobaculum yellowstonensis* strain WP30 produces thioarsenate during
736 respiratory elemental sulfur and As(V) reduction(89). More work is needed to know if the
737 protein complex encoded by operon D interacts with As(III), As(V), or with
738 thiosulfates/polysulfides and enables *P. mercurii* ND132 to respire As. However, it may be
739 responsible for producing the unknown thioarsenic species observed in *P. mercurii* ND132
740 culture media.
741 In As(V) washed cells an operon with homology to the acetoin dehydrogenase complex
742 was upregulated. In batch cultures, this operon was significantly downregulated in all treatments
743 except methionine (Figure S15). The operon is predicted to encode an acetoin dehydrogenase
744 enzyme system (AoDH ES) that catalyzes the conversion of acetoin to acetyl-CoA and
745 acetaldehyde (Figure 8). The AoDH ES contains multiple copies of three enzymatic components:
746 acetoin oxidoreductase (E1), dihydrolipoamide acetyltransferase (E2) and dihydrolipoyl
747 dehydrogenase (E3)(90, 91). The operon (Operon E, Figure 8) encodes AoDH ES homologues
748 annotated as a dihydrolipoamide acetyltransferase (DND132_3103), (PFam PF00198, PF00364,
749 PF02817), an acetoin:2,6-dichlorophenolindophenol oxidoreductase subunit alpha

750 (DND132_3105) (dehydrogenase E1 component, PFam PF00676), acetoin:2,6-
751 dichlorophenolindophenol oxidoreductase subunit beta (DND132_3106) (transketolase central
752 region, PFam PF02779, PF02780), and an acetoin catabolism protein with ATP-NAD/AcoX
753 kinase motifs (PFam PF01513). These proteins also share homology to enzymes in the pyruvate
754 dehydrogenase complex that convert pyruvate into acetyl-CoA by pyruvate decarboxylation(92).
755 The operon is possibly regulated by a sigma(54)-dependent HTH transcriptional regulator
756 (DND132_3102). In closely related *Pseudodesulfovibrio hydrargi* BerOc1 this protein is
757 annotated as an acetoin dehydrogenase operon transcriptional activator AcoR (Uniprot:
758 A0A1J5NC98). No obvious link to As metabolism or resistance could be found. It is possible
759 that this putative AoDH ES operon is upregulated in *P. mercurii* ND132 As(V) washed cells
760 because of cross-reactivity of As with the HTH regulator (DND132_3102) or because of a
761 knock-on effect from other differentially regulated mechanisms.
762
763 **Summary:** The broad research aim of these experiments was to examine transcriptional
764 regulation of *hgcAB* in *Pseudodesulfovibrio mercurii* ND132*,* with a focus on the potential role
765 of an upstream ArsR-like regulator found in *hgc*+ Deltaproteobacteria. Additionally, we
766 examined the relationship between Hg methylation rates in *Pseudodesulfovibrio mercurii* ND132
767 with metabolic activity and *hgcAB* transcriptional activity. We have shown that *hgcAB*
768 expression in *Pseudodesulfovibrio mercurii* ND132 is transcriptionally regulated by an ArsR-like
769 regulator encoded by *arsR2* (DND132_1054) that is responsive to As and SAH. Since *P.*
770 *mercurii* ND132 can reduce As(V) to As(III), and we observed increased *hgcA* and *hgcB*
771 expression when grown with both species, it is likely that As(III) coordinates with ArsR2. The
772 *hgcAB* transcriptional regulator shares homology to other members of the ArsR/SmtB family, but

773 has a distinct four-cysteine motif in its metal(loid) binding site. This homology also distinguishes
774 it from other ArsR family regulators encoded in the genome of *P. mercurii* ND132. Since As(III)
775 preferentially binds to three cysteine residues in ArsR repressors of the *ars* operon, we cannot
776 exclude the possibility that another As species or heavy metal(loid) cation may coordinate with
777 ArsR2 and also control *hgcAB* expression. Although the transcriptional response to As was more
778 pronounced, under some culture conditions methionine and adenosine dialdehyde also
779 significantly increased *arsR2* and *hgcAB* transcription. We attribute this transcriptional response
780 to a build-up in SAH within the cell.

781 The RNA-seq analyses show that *hgcAB* transcription is co-regulated as part of the ArsR
782 regulon with operons that encode As resistance. We also observed significant co-expression of
783 *hgcAB* with genes that encode putative As(V) or polysulfide respiration when *P. mercurii*
784 ND132 is grown with As. These pathways may explain the possible thioarsenic production
785 observed in *P. mercurii* ND132 cultures. This indicates that As biogeochemistry may influence
786 *hgcAB* expression and Hg-methylator activity in some environmental settings. In this study, we
787 did not observe a significant loss in As resistance with a loss in *hgcAB* function in
788 *Pseudodesulfovibrio mercurii* ND132. However, the co-expression and co-localization of *hgcAB*
789 with arsenic resistance genes in some *hgc+* genomes may hold clues to *hgcAB* evolution and
790 possible environmental drivers of horizontal transfer of these genes. More work is needed to
791 tease apart possible overlaps between HgcAB function and arsenic resistance and respiration
792 mechanisms.

793 Results from these experiments do not confirm that higher *hgcAB* expression alone
794 increases MeHg production, but that growth and culture conditions, and the nature of *hgcAB*
795 transcriptional regulation probably all play roles in methylation control. Both As(III) and As(V)

796 impacted Hg methylation and transcription of *hgcAB* and *arsR* in *P. mercurii* ND132, although
797 the impacts were not always coupled. We also observed that metabolic activity and microbial
798 biomass can significantly influence Hg methylation rates in cultures, and counter possible
799 impacts of *hgcAB* activity. Hg methylation rates may also be impacted by HgcAB translation,
800 protein folding, co-factor and membrane insertion, and the methyl donor mechanism. Combining
801 information of *hgcAB* transcription with microbiome composition, metabolic activity, and Hg
802 speciation and geochemistry may help resolve environmental Hg methylation rates. It is
803 therefore important to have accurate and reliable methods for measuring these factors and using
804 multiple parameters when incorporating microbial dynamics into predictive models for Hg
805 methylation.
806

807 **ACKNOWELDGEMENTS**

808 Caitlin Gionfriddo was a Robert and Arlene Kogod Secretarial Scholar with the Smithsonian
809 Environmental Research Center while conducting work described in this manuscript. This work
810 was funded by the U.S. Department of Energy, Office of Science, Office of Biological and
811 Environmental Research, Subsurface Biogeochemical Research (SBR) Program, and is a product
812 of the Critical Interfaces Science Focus Area at Oak Ridge National Laboratory, which is
813 managed by UT-Battelle, LLC under Contract No. DE-AC05-00OR22725 with the U.S.
814 Department of Energy. The As speciation analysis was performed by Brooks Applied Labs and
815 we thank Ben Wozniak and Collette Machado for technical support. The RNA-seq transcriptome
816 analyses were performed at Azenta US Inc. and we thank Andrew Corbin and Eric Danzeisen for
817 technical support.
818

819 **DATA AVAILABILITY STATEMENT**

820 The transcriptomic sequencing data is publicly available through KBase narrative

821 (https://narrative.kbase.us/narrative/124642).

822

823 **SUPPLEMENTARY MATERIAL**

824 See attached document of supplementary methods, tables, and figures.

825

826 **REFERENCES**

827 1. Branfireun BA, Cosio C, Poulain AJ, Riise G, Bravo AG. 2020. Mercury cycling in

828 freshwater systems-An updated conceptual model. Science of the Total Environment

829 745:140906.

830 2. Parks JM, Johs A, Podar M, Bridou R, Hurt RA, Smith SD, Tomanicek SJ, Qian Y,

831 Brown SD, Brandt CC. 2013. The genetic basis for bacterial mercury methylation.

832 Science 339:1332-1335.

833 3. Podar M, Gilmour CC, Brandt CC, Soren A, Brown SD, Crable BR, Palumbo AV,

834 Somenahally AC, Elias DA. 2015. Global prevalence and distribution of genes and

835 microorganisms involved in mercury methylation. Sci Adv 1:e1500675.

836 4. McDaniel EA, Peterson B, Stevens SL, Tran PQ, Anantharaman K, McMahon K. 2020.

837 Expanded Phylogenetic Diversity and Metabolic Flexibility of Microbial Mercury

838 Methylation. BioRxiv.

839 5. Gilmour CC, Podar M, Bullock AL, Graham AM, Brown SD, Somenahally AC, Johs A,

840 Hurt Jr RA, Bailey KL, Elias DA. 2013. Mercury methylation by novel microorganisms

841 from new environments. Environmental science & technology 47:11810-11820.

842 6. Gionfriddo CM, Wymore AM, Jones DS, Wilpiszeski RL, Lynes MM, Christensen GA,
843 Soren A, Gilmour CC, Podar M, Elias DA. 2020. An Improved hgcAB Primer Set and
844 Direct High-Throughput Sequencing Expand Hg-Methylator Diversity in Nature.
845 Frontiers in Microbiology 11.
846 7. Capo E, Peterson BD, Kim M, Jones DS, Acinas SG, Amyot M, Bertilsson S, Björn E,
847 Buck M, Cosio C. 2022. A consensus protocol for the recovery of mercury methylation
848 genes from metagenomes. Molecular Ecology Resources.
849 8. Goñi-Urriza M, Klopp C, Ranchou-Peyruse M, Ranchou-Peyruse A, Monperrus M,
850 Khalfaoui-Hassani B, Guyoneaud R. 2019. Genome insights of mercury methylation
851 among Desulfovibrio and Pseudodesulfovibrio strains. Research in microbiology.
852 9. Gilmour CC, Soren AB, Gionfriddo CM, Podar M, Wall JD, Brown SD, Michener JK,
853 Urriza MSG, Elias DA. 2021. Pseudodesulfovibrio mercurii sp. nov., a mercury-
854 methylating bacterium isolated from sediment. International Journal of Systematic and
855 Evolutionary Microbiology 71:004697.
856 10. Ranchou-Peyruse M, Goñi-Urriza M, Guignard M, Goas M, Ranchou-Peyruse A,
857 Guyoneaud R. 2018. Pseudodesulfovibrio hydrargyri sp. nov., a mercury-methylating
858 bacterium isolated from a brackish sediment. International Journal of Systematic and
859 Evolutionary Microbiology 68:1461-1466.
860 11. Gionfriddo C, Capo E, Peterson B, Lin H, Jones D, Bravo A. 2021. Hg-cycling
861 Microorganisms in Aquatic and Terrestrial Ecosystems Database v1. 01142021.
862 12. Gilmour CC, Bullock AL, McBurney A, Podar M, Elias DA. 2018. Robust Mercury
863 Methylation across Diverse Methanogenic Archaea. mBio 9.

864 13. King JK, Kostka JE, Frischer ME, Saunders FM. 2000. Sulfate-reducing bacteria
865 methylate mercury at variable rates in pure culture and in marine sediments. Applied and
866 Environmental Microbiology 66:2430-2437.
867 14. King J, Kostka J, Frischer M, Saunders FM, Jahnke R. 2001. A Quantitative Relationship
868 that Demonstrates Mercury Methylation Rates in Marine Sediments Are. Environmental
869 science & technology 35:2491.
870 15. Date SS, Parks JM, Rush KW, Wall JD, Ragsdale SW, Johs A. 2019. Kinetics of
871 enzymatic mercury methylation at nanomolar concentrations catalyzed by HgcAB.
872 Applied and environmental microbiology 85:e00438-19.
873 16. Schaefer JK, Rocks SS, Zheng W, Liang L, Gu B, Morel FM. 2011. Active transport,
874 substrate specificity, and methylation of Hg (II) in anaerobic bacteria. Proceedings of the
875 National Academy of Sciences 108:8714-8719.
876 17. Graham AM, Bullock AL, Maizel AC, Elias DA, Gilmour CC. 2012. Detailed assessment
877 of the kinetics of Hg-cell association, Hg methylation, and methylmercury degradation in
878 several Desulfovibrio species. Applied and environmental microbiology 78:7337-7346.
879 18. Cooper CJ, Zheng K, Rush KW, Johs A, Sanders BC, Pavlopoulos GA, Kyrpides NC,
880 Podar M, Ovchinnikov S, Ragsdale SW. 2020. Structure determination of the HgcAB
881 complex using metagenome sequence data: insights into microbial mercury methylation.
882 Communications biology 3:1-9.
883 19. Smith SD, Bridou R, Johs A, Parks JM, Elias DA, Hurt Jr RA, Brown SD, Podar M, Wall
884 JD. 2015. Site-directed mutagenesis of HgcA and HgcB reveals amino acid residues
885 important for mercury methylation. Applied and environmental microbiology 81:3205-
886 3217.

887 20. Zhang Y, Rodionov DA, Gelfand MS, Gladyshev VN. 2009. Comparative genomic
888 analyses of nickel, cobalt and vitamin B12 utilization. BMC genomics 10:1-26.
889 21. Bridwell-Rabb J, Drennan CL. 2017. Vitamin B12 in the spotlight again. Current opinion
890 in chemical biology 37:63-70.
891 22. Goulding CW, Postigo D, Matthews RG. 1997. Cobalamin-dependent methionine
892 synthase is a modular protein with distinct regions for binding homocysteine,
893 methyltetrahydrofolate, cobalamin, and adenosylmethionine. Biochemistry 36:8082-
894 8091.
895 23. Ragsdale S, Lindahl P, Münck E. 1987. Mössbauer, EPR, and optical studies of the
896 corrinoid/iron-sulfur protein involved in the synthesis of acetyl coenzyme A by
897 Clostridium thermoaceticum. Journal of Biological Chemistry 262:14289-14297.
898 24. Choi SC, Chase T, Bartha R. 1994a. Enzymatic Catalysis of Mercury Methylation by
899 Desulfovibrio-Desulfuricans LS. Applied and environmental microbiology 60:1342-
900 1346.
901 25. Choi SC, Chase T, Bartha R. 1994b. Metabolic Pathways Leading to Mercury
902 Methylation in *Desulfovibrio-desulfuricans* LS. Applied and environmental microbiology
903 60:4072-4077.
904 26. Siciliano SD, Lean DRS. 2002. Methyltransferase: An enzyme assay for microbial
905 methylmercury formation in acidic soils and sediments. Environmental Toxicology and
906 Chemistry 21:1184-1190.
907 27. Zhou J, Riccardi D, Beste A, Smith JC, Parks JM. 2014. Mercury methylation by HgcA:
908 theory supports carbanion transfer to Hg (II). Inorganic chemistry 53:772-777.

28. Qian C, Chen H, Johs A, Lu X, An J, Pierce EM, Parks JM, Elias DA, Hettich RL, Gu B. 2018. Quantitative proteomic analysis of biological processes and responses of the bacterium Desulfovibrio desulfuricans ND132 upon deletion of its mercury methylation genes. Proteomics 18:1700479.

29. Goñi-Urriza M, Corsellis Y, Lanceleur L, Tessier E, Gury J, Monperrus M, Guyoneaud R. 2015. Relationships between bacterial energetic metabolism, mercury methylation potential, and hgcA/hgcB gene expression in Desulfovibrio dechloroacetivorans BerOc1. Environmental Science and Pollution Research 22:13764-13771.

30. Gilmour CC, Elias DA, Kucken AM, Brown SD, Palumbo AV, Schadt CW, Wall JD. 2011. Sulfate-reducing bacterium Desulfovibrio desulfuricans ND132 as a model for understanding bacterial mercury methylation. Applied and environmental microbiology 77:3938-3951.

31. Grégoire DS, Poulain AJ. 2018. Shining light on recent advances in microbial mercury cycling. Facets 3:858-879.

32. Rathore SS, Schwartz GE, Brooks SC, Painter SL. 2022. Joint estimation of biogeochemical model parameters from multiple experiments: A bayesian approach applied to mercury methylation. Environmental Modelling & Software:105453.

33. Bravo AG, Cosio C. 2019. Biotic formation of methylmercury: A bio–physico–chemical conundrum. Limnology and Oceanography.

34. Hsu-Kim H, Kucharzyk KH, Zhang T, Deshusses MA. 2013. Mechanisms regulating mercury bioavailability for methylating microorganisms in the aquatic environment: A critical review. Environmental Science & Technology 47:2441-2456.

931 35. Christensen GA, Gionfriddo CM, King AJ, Moberly JG, Miller CL, Somenahally AC,
932 Callister SJ, Brewer H, Podar M, Brown SD. 2019. Determining the Reliability of
933 Measuring Mercury Cycling Gene Abundance with Correlations with Mercury and
934 Methylmercury Concentrations. Environmental science & technology 53:8649-8663.
935 36. Schaefer JK, Kronberg RM, Björn E, Skyllberg U. 2020. Anaerobic guilds responsible
936 for mercury methylation in boreal wetlands of varied trophic status serving as either a
937 methylmercury source or sink. Environmental microbiology 22:3685-3699.
938 37. Rocca JD, Hall EK, Lennon JT, Evans SE, Waldrop MP, Cotner JB, Nemergut DR,
939 Graham EB, Wallenstein MD. 2015. Relationships between protein-encoding gene
940 abundance and corresponding process are commonly assumed yet rarely observed. The
941 ISME journal 9:1693-1699.
942 38. Liu Y-R, Yang Z, Zhou X, Qu X, Li Z, Zhong H. 2019. Overlooked role of putative non-
943 Hg methylators in predicting methylmercury production in paddy soils. Environmental
944 Science & Technology 53:12330-12338.
945 39. Capo E, Feng C, Bravo AG, Bertilsson S, Soerensen AL, Pinhassi J, Buck M, Karlsson
946 C, Hawkes J, Björn E. 2022. Abundance and expression of hgcAB genes and mercury
947 availability jointly explain methylmercury formation in stratified brackish waters.
948 bioRxiv.
949 40. Bouchet S, Goñi-Urriza M, Monperrus M, Guyoneaud Rm, Fernandez P, Heredia C,
950 Tessier E, Gassie C, Point D, Guédron S. 2018. Linking microbial activities and low-
951 molecular-weight thiols to Hg methylation in biofilms and periphyton from high-altitude
952 tropical lakes in the Bolivian Altiplano. Environmental science & technology 52:9758-
953 9767.

954 41. Lin H, Ascher DB, Myung Y, Lamborg CH, Hallam SJ, Gionfriddo CM, Holt KE,
955 Moreau JW. 2020. Mercury methylation by metabolically versatile and cosmopolitan
956 marine bacteria. bioRxiv.
957 42. Peterson BD, McDaniel EA, Schmidt AG, Lepak RF, Janssen SE, Tran PQ, Marick RA,
958 Ogorek JM, DeWild JF, Krabbenhoft DP. 2020. Mercury methylation genes identified
959 across diverse anaerobic microbial guilds in a eutrophic sulfate-enriched lake.
960 Environmental Science & Technology 54:15840-15851.
961 43. Gionfriddo CM, Stott MB, Power JF, Ogorek JM, Krabbenhoft DP, Wick R, Holt K,
962 Chen L-X, Thomas BC, Banfield JF. 2020. Genome-resolved metagenomics and detailed
963 geochemical speciation analyses yield new insights into microbial mercury cycling in
964 geothermal springs. Applied and environmental microbiology 86.
965 44. Leyn SA, Suvorova IA, Kholina TD, Sherstneva SS, Novichkov PS, Gelfand MS,
966 Rodionov DA. 2014. Comparative Genomics of Transcriptional Regulation of
967 Methionine Metabolism in Proteobacteria. PLOS ONE 9:e113714.
968 45. Novichkov PS, Li X, Kuehl JV, Deutschbauer AM, Arkin AP, Price MN, Rodionov DA.
969 2014. Control of methionine metabolism by the SahR transcriptional regulator in
970 Proteobacteria. Environ Microbiol 16:1-8.
971 46. Li X, Krumholz LR. 2007. Regulation of arsenate resistance in Desulfovibrio
972 desulfuricans G20 by an arsRBCC operon and an arsC gene. J Bacteriol 189:3705-11.
973 47. Ekstrom EB, Morel FMM. 2008. Cobalt limitation of growth and mercury methylation in
974 sulfate-reducing bacteria. Environmental science & technology 42:93-99.
975 48. Smith SD. 2015. Protein components of the microbial mercury methylation
976 pathwayUniversity of Missouri--Columbia.

977 49. Brown SD, Gilmour CC, Kucken AM, Wall JD, Elias DA, Brandt CC, Podar M,
978 Chertkov O, Held B, Bruce DC. 2011. Genome sequence of the mercury-methylating
979 strain Desulfovibrio desulfuricans ND132. Am Soc Microbiol.
980 50. Walker CB, He Z, Yang ZK, Ringbauer Jr JA, He Q, Zhou J, Voordouw G, Wall JD,
981 Arkin AP, Hazen TC. 2009. The electron transfer system of syntrophically grown
982 Desulfovibrio vulgaris. Journal of bacteriology 191:5793-5801.
983 51. Graham AM, Aiken GR, Gilmour CC. 2012. Dissolved Organic Matter Enhances
984 Microbial Mercury Methylation Under Sulfidic Conditions. Environmental Science &
985 Technology 46:2715-2723.
986 52. Arkin AP, Cottingham RW, Henry CS, Harris NL, Stevens RL, Maslov S, Dehal P, Ware
987 D, Perez F, Canon S, Sneddon MW, Henderson ML, Riehl WJ, Murphy-Olson D, Chan
988 SY, Kamimura RT, Kumari S, Drake MM, Brettin TS, Glass EM, Chivian D, Gunter D,
989 Weston DJ, Allen BH, Baumohl J, Best AA, Bowen B, Brenner SE, Bun CC, Chandonia
990 J-M, Chia J-M, Colasanti R, Conrad N, Davis JJ, Davison BH, DeJongh M, Devoid S,
991 Dietrich E, Dubchak I, Edirisinghe JN, Fang G, Faria JP, Frybarger PM, Gerlach W,
992 Gerstein M, Greiner A, Gurtowski J, Haun HL, He F, Jain R, et al. 2018. KBase: The
993 United States Department of Energy Systems Biology Knowledgebase. Nature
994 Biotechnology 36:566-569.
995 53. Bolger AM, Lohse M, Usadel B. 2014. Trimmomatic: a flexible trimmer for Illumina
996 sequence data. Bioinformatics 30:2114-2120.
997 54. Kim D, Paggi JM, Park C, Bennett C, Salzberg SL. 2019. Graph-based genome
998 alignment and genotyping with HISAT2 and HISAT-genotype. Nature Biotechnology
999 37:907-915.

1000 55. Pertea M, Pertea GM, Antonescu CM, Chang T-C, Mendell JT, Salzberg SL. 2015.
1001 StringTie enables improved reconstruction of a transcriptome from RNA-seq reads.
1002 Nature Biotechnology 33:290-295.
1003 56. Love MI, Huber W, Anders S. 2014. Moderated estimation of fold change and dispersion
1004 for RNA-seq data with DESeq2. Genome Biology 15:550.
1005 57. Afgan E, Baker D, Batut B, van den Beek M, Bouvier D, Čech M, Chilton J, Clements D,
1006 Coraor N, Grüning BA, Guerler A, Hillman-Jackson J, Hiltemann S, Jalili V, Rasche H,
1007 Soranzo N, Goecks J, Taylor J, Nekrutenko A, Blankenberg D. 2018. The Galaxy
1008 platform for accessible, reproducible and collaborative biomedical analyses: 2018 update.
1009 Nucleic Acids Research 46:W537-W544.
1010 58. Mirdita M, Schütze K, Moriwaki Y, Heo L, Ovchinnikov S, Steinegger M. 2022.
1011 ColabFold: making protein folding accessible to all. Nature Methods 19:679-682.
1012 59. Jumper J, Evans R, Pritzel A, Green T, Figurnov M, Ronneberger O, Tunyasuvunakool
1013 K, Bates R, Žídek A, Potapenko A, Bridgland A, Meyer C, Kohl SAA, Ballard AJ,
1014 Cowie A, Romera-Paredes B, Nikolov S, Jain R, Adler J, Back T, Petersen S, Reiman D,
1015 Clancy E, Zielinski M, Steinegger M, Pacholska M, Berghammer T, Bodenstein S, Silver
1016 D, Vinyals O, Senior AW, Kavukcuoglu K, Kohli P, Hassabis D. 2021. Highly accurate
1017 protein structure prediction with AlphaFold. Nature 596:583-589.
1018 60. Mirdita M, Steinegger M, Söding J. 2019. MMseqs2 desktop and local web server app for
1019 fast, interactive sequence searches. Bioinformatics 35:2856-2858.
1020 61. Mitchell AL, Almeida A, Beracochea M, Boland M, Burgin J, Cochrane G, Crusoe MR,
1021 Kale V, Potter SC, Richardson LJ, Sakharova E, Scheremetjew M, Korobeynikov A,

1022 Shlemov A, Kunyavskaya O, Lapidus A, Finn RD. 2020. MGnify: the microbiome
1023 analysis resource in 2020. Nucleic Acids Research 48:D570-D578.
1024 62. Evans R, O'Neill M, Pritzel A, Antropova N, Senior A, Green T, Žídek A, Bates R,
1025 Blackwell S, Yim J, Ronneberger O, Bodenstein S, Zielinski M, Bridgland A, Potapenko
1026 A, Cowie A, Tunyasuvunakool K, Jain R, Clancy E, Kohli P, Jumper J, Hassabis D.
1027 2022. Protein complex prediction with AlphaFold-Multimer. bioRxiv
1028 doi:10.1101/2021.10.04.463034:2021.10.04.463034.
1029 63. Team RC. 2013. R: A language and environment for statistical computing.
1030 64. Busenlehner LS, Pennella MA, Giedroc DP. 2003. The SmtB/ArsR family of
1031 metalloregulatory transcriptional repressors: Structural insights into prokaryotic metal
1032 resistance. FEMS Microbiol Rev 27:131-43.
1033 65. Andres J, Bertin PN. 2016. The microbial genomics of arsenic. FEMS Microbiology
1034 Reviews 40:299-322.
1035 66. Chen J, Madegowda M, Bhattacharjee H, Rosen BP. 2015. ArsP: a methylarsenite efflux
1036 permease. Molecular Microbiology 98:625-635.
1037 67. Chen J, Zhang J, Rosen BP. 2019. Role of ArsEFG in Roxarsone and Nitarsone
1038 Detoxification and Resistance. Environmental Science & Technology 53:6182-6191.
1039 68. Rawle R, Saley TC, Kang Y-S, Wang Q, Walk S, Bothner B, McDermott TR. 2021.
1040 Introducing the ArsR-Regulated Arsenic Stimulon. Frontiers in Microbiology 12.
1041 69. Qin J, Rosen BP, Zhang Y, Wang G, Franke S, Rensing C. 2006. Arsenic detoxification
1042 and evolution of trimethylarsine gas by a microbial arsenite S-
1043 adenosylmethionine methyltransferase. Proceedings of the National Academy of Sciences
1044 103:2075-2080.

1045 70. Woodcroft BJ, Singleton CM, Boyd JA, Evans PN, Emerson JB, Zayed AAF, Hoelzle
1046 RD, Lamberton TO, McCalley CK, Hodgkins SB, Wilson RM, Purvine SO, Nicora CD,
1047 Li C, Frolking S, Chanton JP, Crill PM, Saleska SR, Rich VI, Tyson GW. 2018.
1048 Genome-centric view of carbon processing in thawing permafrost. Nature 560:49-54.
1049 71. Haas S, Desai DK, LaRoche J, Pawlowicz R, Wallace DWR. 2019. Geomicrobiology of
1050 the carbon, nitrogen and sulphur cycles in Powell Lake: a permanently stratified water
1051 column containing ancient seawater. Environmental Microbiology 21:3927-3952.
1052 72. Qiu YL, Kuang XZ, Shi XS, Yuan XZ, Guo RB. 2014. Paludibacter jiangxiensis sp. nov.,
1053 a strictly anaerobic, propionate-producing bacterium isolated from rice paddy field. Arch
1054 Microbiol 196:149-55.
1055 73. Anantharaman K, Brown CT, Hug LA, Sharon I, Castelle CJ, Probst AJ, Thomas BC,
1056 Singh A, Wilkins MJ, Karaoz U. 2016. Thousands of microbial genomes shed light on
1057 interconnected biogeochemical processes in an aquifer system. Nature communications
1058 7:13219.
1059 74. Giloteaux L, Holmes DE, Williams KH, Wrighton KC, Wilkins MJ, Montgomery AP,
1060 Smith JA, Orellana R, Thompson CA, Roper TJ, Long PE, Lovley DR. 2013.
1061 Characterization and transcription of arsenic respiration and resistance genes during in
1062 situ uranium bioremediation. The ISME Journal 7:370-383.
1063 75. Prabaharan C, Kandavelu P, Packianathan C, Rosen BP, Thiyagarajan S. 2019. Structures
1064 of two ArsR As(III)-responsive transcriptional repressors: Implications for the
1065 mechanism of derepression. Journal of Structural Biology 207:209-217.

1066 76. Shi W, Dong J, Scott RA, Ksenzenko MY, Rosen BP. 1996. The Role of Arsenic-Thiol
1067 Interactions in Metalloregulation of the ars Operon (∗). Journal of Biological Chemistry
1068 271:9291-9297.
1069 77. Packianathan C, Kandavelu P, Rosen BP. 2018. The Structure of an As (III) S-
1070 adenosylmethionine methyltransferase with 3-coordinately bound As (III) depicts the first
1071 step in catalysis. Biochemistry 57:4083-4092.
1072 78. Rush K. 2018. Expression and characterization of HgcA and HgcB, two proteins
1073 involved in methylmercury biosynthesis.
1074 79. Barrouilhet S, Monperrus M, Tessier E, Khalfaoui-Hassani B, Guyoneaud R, Isaure M-P,
1075 Goñi-Urriza M. 2021. Effect of Exogenous and Endogenous Sulfide on The Production
1076 and The Export of Methylmercury by Sulfate Reducing Bacteria.
1077 80. Benoit JM, Gilmour CC, Mason RP. 2001. The influence of sulfide on solid phase
1078 mercury bioavailability for methylation by pure cultures of *Desulfobulbus propionicus*
1079 (1pr3). Environmental Science & Technology 35:127-132.
1080 81. Mija A, Jules M B, Alexandre J P. 2022. Arsenate decreases production of
1081 methylmercury across increasing sulfate concentration amendments in freshwater lake
1082 sediments. Environmental Science: Processes & Impacts doi:10.1039/D1EM00543J.
1083 82. Glasser NR, Oyala PH, Osborne TH, Santini JM, Newman DK. 2018. Structural and
1084 mechanistic analysis of the arsenate respiratory reductase provides insight into
1085 environmental arsenic transformations. Proceedings of the National Academy of Sciences
1086 115:E8614-E8623.
1087 83. Stolz JF, Basu P. 2018. Unraveling the inner workings of respiratory arsenate reductase.
1088 Proceedings of the National Academy of Sciences 115:9051-9053.

1089 84. Malasarn D, Keeffe JR, Newman DK. 2008. Characterization of the Arsenate Respiratory
1090 Reductase from Shewanella sp. Strain ANA-3. Journal of Bacteriology 190:135-
1091 142.
1092 85. Tsuchiya T, Ehara A, Kasahara Y, Hamamura N, Amachi S, Zhou N-Y. 2019. Expression
1093 of Genes and Proteins Involved in Arsenic Respiration and Resistance in Dissimilatory
1094 Arsenate-Reducing Geobacter sp. Strain OR-1. Applied and Environmental
1095 Microbiology 85:e00763-19.
1096 86. Richey C, Chovanec P, Hoeft SE, Oremland RS, Basu P, Stolz JF. 2009. Respiratory
1097 arsenate reductase as a bidirectional enzyme. Biochemical and Biophysical Research
1098 Communications 382:298-302.
1099 87. Jormakka M, Yokoyama K, Yano T, Tamakoshi M, Akimoto S, Shimamura T, Curmi P,
1100 Iwata S. 2008. Molecular mechanism of energy conservation in polysulfide respiration.
1101 Nat Struct Mol Biol 15:730-7.
1102 88. Wang S, Jiang L, Hu Q, Liu X, Yang S, Shao Z. 2021. Elemental sulfur reduction by a
1103 deep-sea hydrothermal vent Campylobacterium Sulfurimonas sp. NW10. Environ
1104 Microbiol 23:965-979.
1105 89. Jay ZJ, Beam JP, Dohnalkova A, Lohmayer R, Bodle B, Planer-Friedrich B, Romine M,
1106 Inskeep WP. 2015. Pyrobaculum yellowstonensis Strain WP30 Respires on Elemental
1107 Sulfur and/or Arsenate in Circumneutral Sulfidic Geothermal Sediments of Yellowstone
1108 National Park. Applied and environmental microbiology 81:5907-5916.
1109 90. Oppermann FB, Schmidt B, Steinbüchel A. 1991. Purification and characterization of
1110 acetoin:2,6-dichlorophenolindophenol oxidoreductase, dihydrolipoamide dehydrogenase,

1111 and dihydrolipoamide acetyltransferase of the Pelobacter carbinolicus acetoin
1112 dehydrogenase enzyme system. Journal of Bacteriology 173:757-767.
1113 91. Oppermann FB, Steinbüchel A. 1994. Identification and molecular characterization of the
1114 aco genes encoding the Pelobacter carbinolicus acetoin dehydrogenase enzyme system.
1115 Journal of Bacteriology 176:469-485.
1116 92. de Kok A, Hengeveld AF, Martin A, Westphal AH. 1998. The pyruvate dehydrogenase
1117 multi-enzyme complex from Gram-negative bacteria. Biochimica et Biophysica Acta
1118 (BBA) - Protein Structure and Molecular Enzymology 1385:353-366.
1119 93. Harrison KJ, Crécy-Lagard Vd, Zallot R. 2017. Gene Graphics: a genomic neighborhood
1120 data visualization web application. Bioinformatics 34:1406-1408.
1121 94. Sprouffske K, Wagner A. 2016. Growthcurver: an R package for obtaining interpretable
1122 metrics from microbial growth curves. BMC Bioinformatics 17:172.
1123
1124

1125 **MAIN FIGURES**

1126

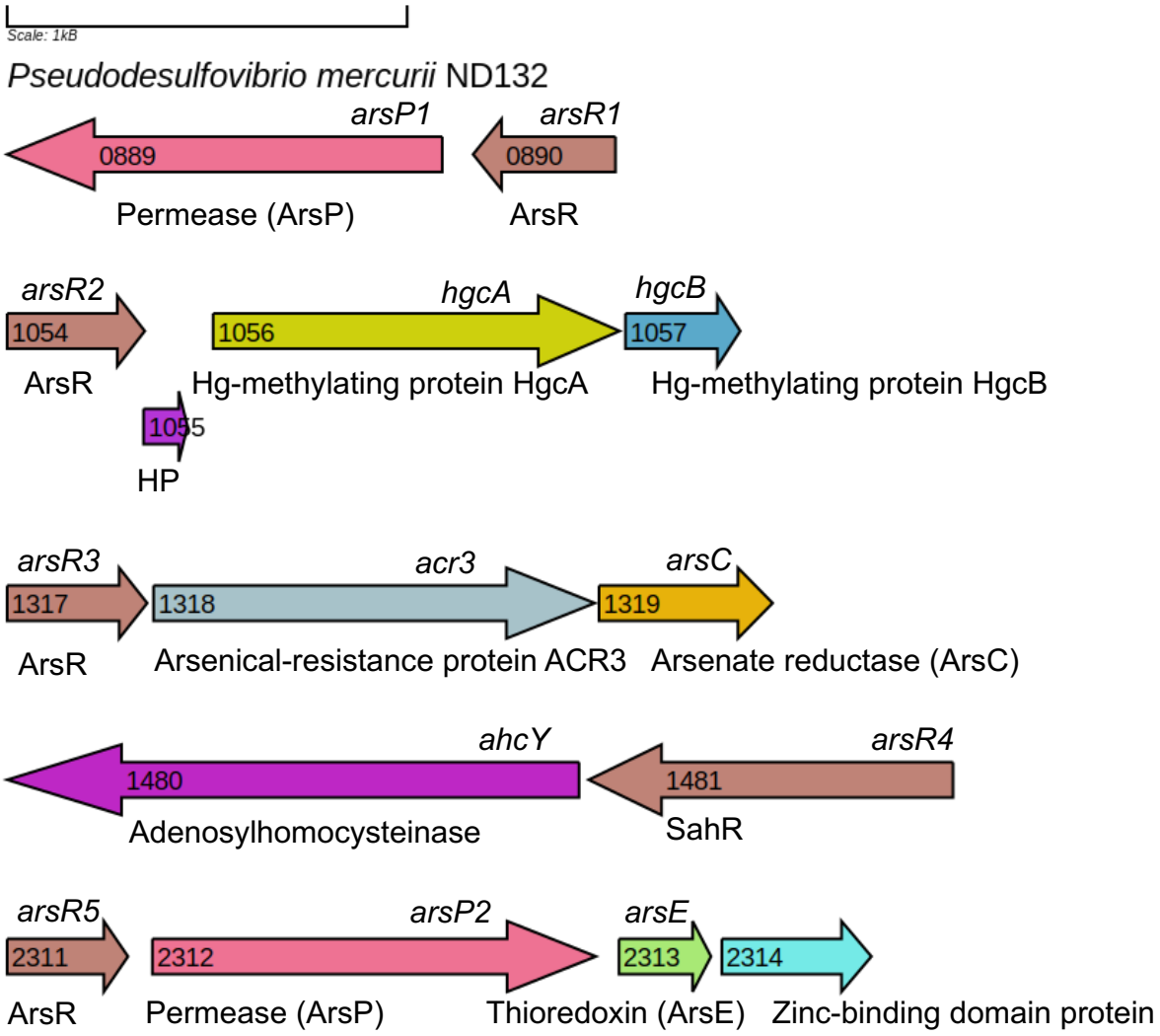

1127

1128 Figure 1. ArsR/SmtB family transcriptional regulators encoded in the genome of

1129 *Pseudodesulfovibrio mercurii* ND132. The five *arsR* genes are numbered by order of appearance

1130 in genome, with gene ID in arrow (e.g. HgcA enoded by DND132_1056), gene orientation

1131 shown by arrows, and color coded by protein family. Figure made using Gene Graphics(93).

1132

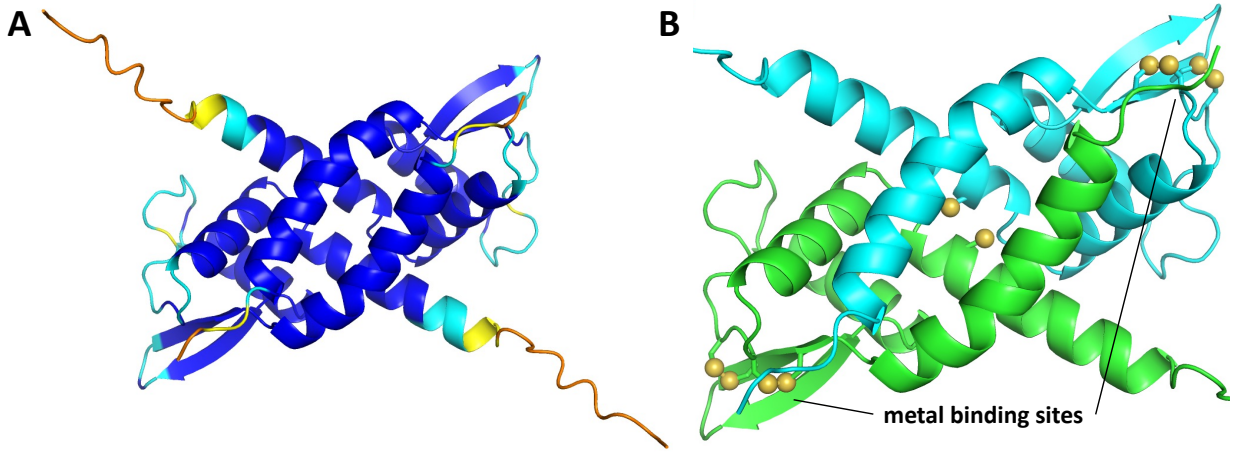

Figure 2. (A) AlphaFold2 model of the putative ArsR-like transcriptional regulator encoded by *arsR2* (Uniprot ID: F0JBE8) and co-localized with *hgcAB* in the genome of *Pseudodesulfovibrio mercurii* ND132. The model is colored by model confidence (i.e., predicted LDDT score). Dark blue = very high confidence (pLDDT > 90), cyan = confident (90 > pLDDT > 70), yellow = low confidence (70 > pLDDT > 50), and orange = very low confidence (pLDDT < 50). (B) Close-up view colored by chain with cysteine residues shown in the ball-and-stick representation.

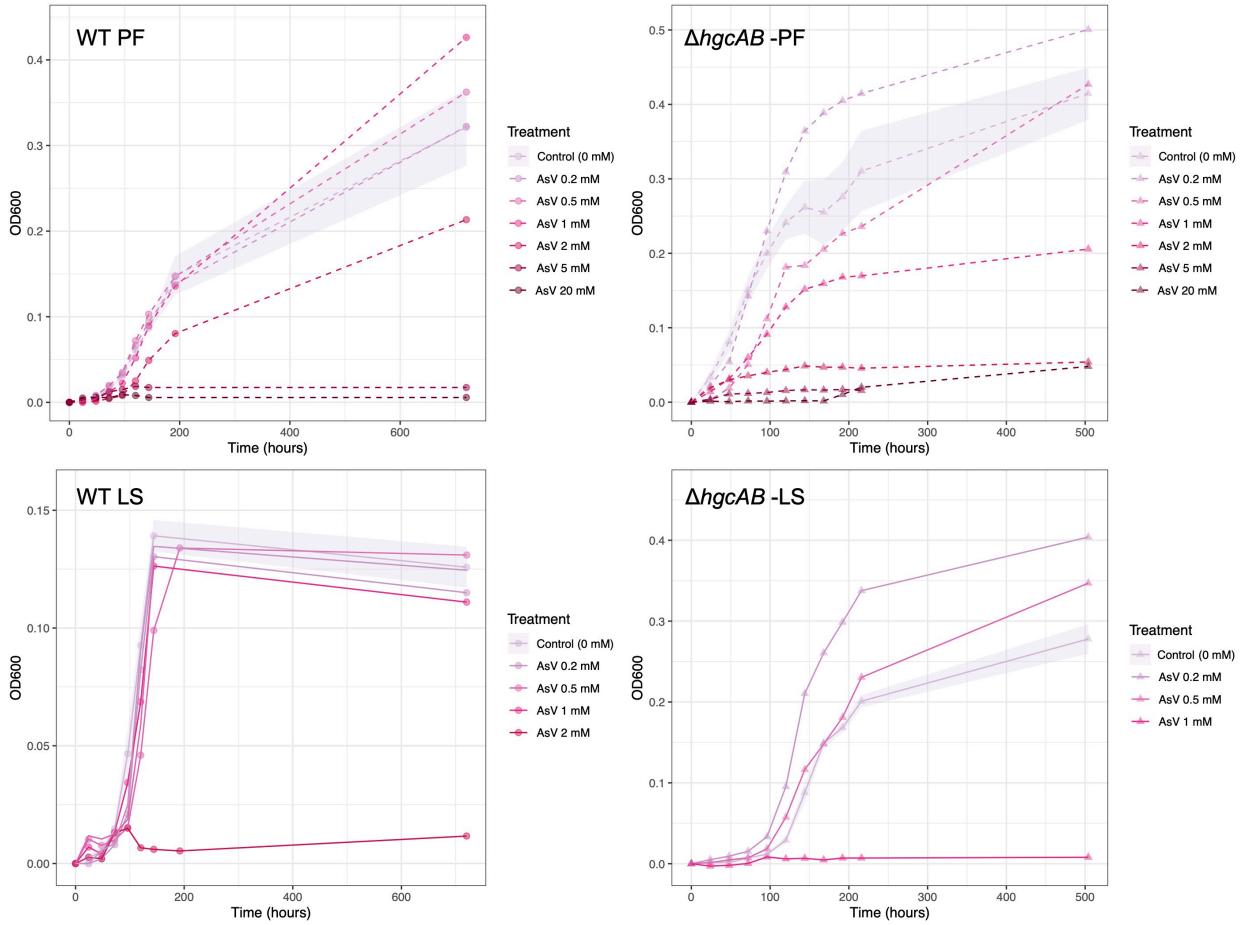

1141

1142 Figure 3. Growth assay tests of arsenate toxicity to *Pseudodesulfovibrio mercurii* ND132 wild-

1143 type (WT) and *hgcAB* deletion mutant (Δ*hgcAB*) in defined CCM media with pyruvate-fumarate

1144 (PF) or lactate-sulfate (LS) and sodium arsenate, As(V). Growth curves fitted to optical density

1145 measured at 600 nm (OD_{600}) absorbance of biological triplicates using 'ggplot' and 'dplyr' in R.

1146 Shaded area shows the standard error of average OD_{600} measurements for control replicates.

1147

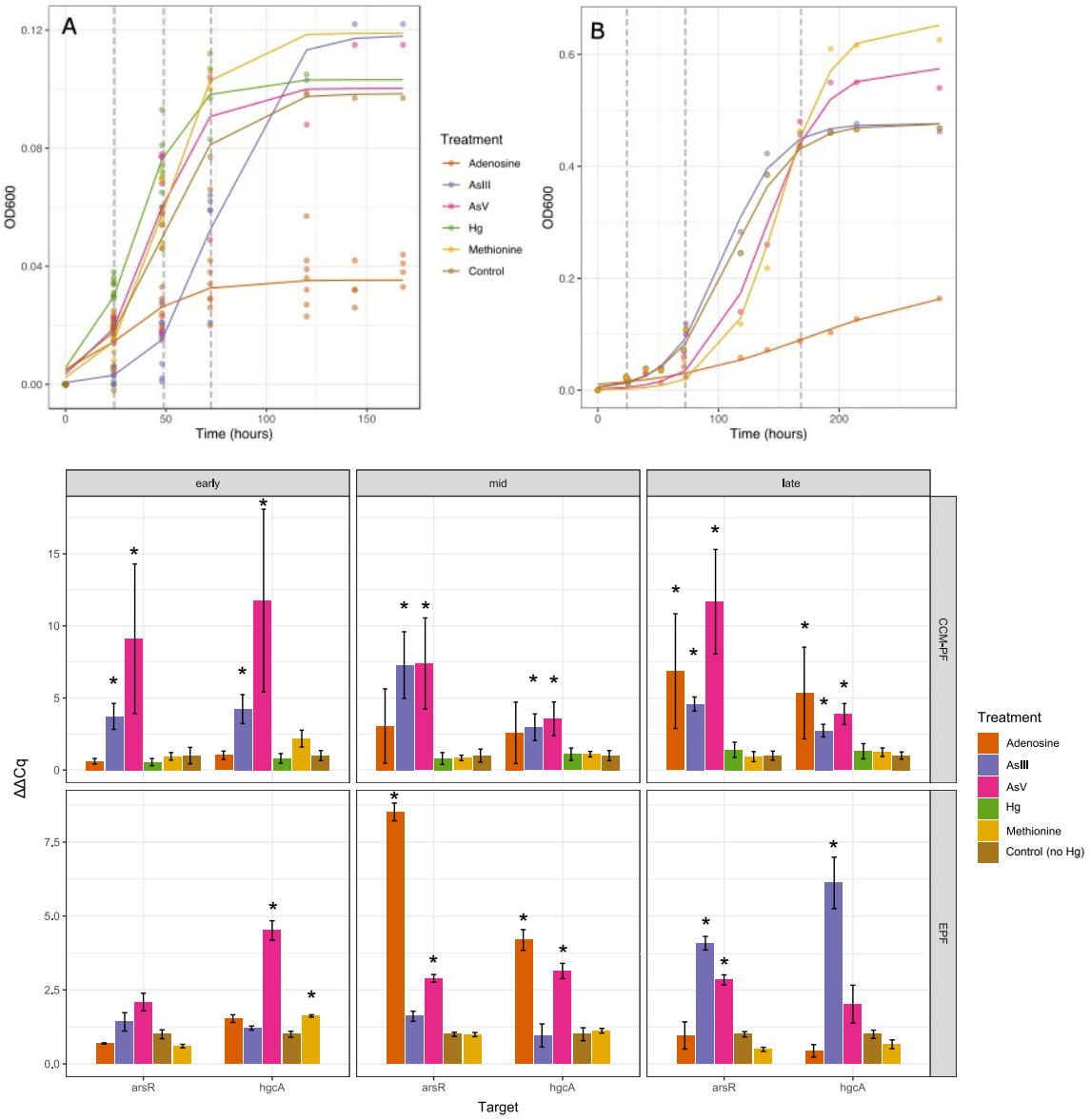

1148

1149 Figure 4. Regulation of *arsR* and *hgcA* expression in wild type *Pseudodesulfovibrio mercurii*

1150 ND132. Top: Growth curves of for cell grown in defined CCM-PF (A) and enriched EPF media

1151 (B) with various potential transcriptional regulators. Growth plotted as change in optical density

1152 at 600 nm absorbance (OD_{600}) from inoculation at T_0, using R program, Growthcurver(94). Gray

1153 dashed lines indicate when cells were harvested for RNA extraction for qPCR at early, mid, and

1154 late exponential growth. Bottom: Relative expression (ΔΔCq) of *arsR2* (DND132_1054) and

1155 *hgcA* (DND132_1056) from qPCR of cDNA (from RNA). Expression of the target genes was

1156 normalized to three housekeeping genes (*gyrA*, *gyrB*, *recA*) and to control (i.e., culture with no
1157 treatment). Treatments: 0.1 mM (CCM and EPF) adenosine-2',3'-dialdehyde, 0.2 mM (CCM)
1158 and 0.02 mM sodium arsenite, 2.0 mM (CCM) and 0.2 mM (EPF) sodium arsenate, 1.0 mM
1159 HgCl (CCM only), 1.0 mM (CCM and EPF) methionine. Stars indicate significant difference
1160 between ΔΔCq of treatment compared to control (z-Test, $p < 0.05$). qPCR was performed on
1161 biological triplicate cultures (CCM) and single culture (EPF) and included three analytical
1162 replicates per cDNA sample.
1163
1164

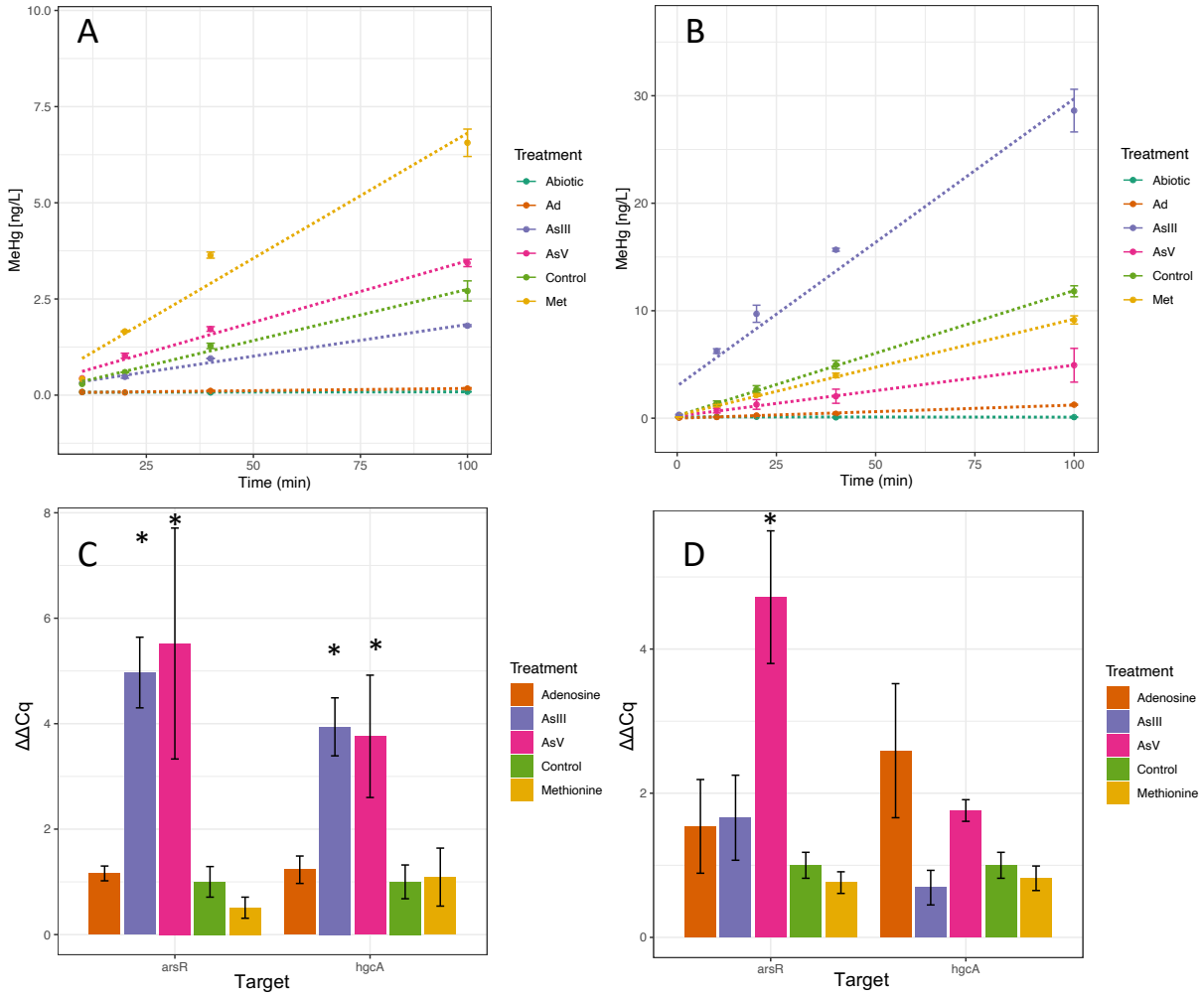

Figure 5. Impact of potential *hgcA* transcription regulators on MeHg production by *Pseudodesulfovibrio mercurii* ND132. Top: MeHg production in washed-cell (A) and batch cultures (B) with treatments: 0.1 mM adenosine-2',3'-dialdehyde, 0.02 mM sodium arsenite, 0.2 mM sodium arsenate, 1.0 mM methionine, control (cells in unamended washed buffer or EPF media), and abiotic (no cells, unamended wash buffer or EPF media). Linear regression fit to data using R. Hg methylation assays were performed in triplicates, with sampling at 0, 10, 20, 40, 100 minutes after being spiked with 1 nM of ^{201}HgCl. Error bars represent +/-1 standard error of the mean. Cells were harvested from assays at t = 100 minutes for qPCR of cDNA (from

1174 RNA) to measure normalized expression (ΔΔCq) of *arsR* (DND132_1054) and *hgcA*

1175 (DND132_1056) in washed cells (C) and batch culture (D). Expression normalized to three

1176 housekeeping genes (*gyrA*, *gyrB*, *recA*) and control (Supp. Methods 1.1). Stars indicate

1177 significant difference between ΔΔCq of treatment compared to control (z-Test, $p < 0.05$).

1178

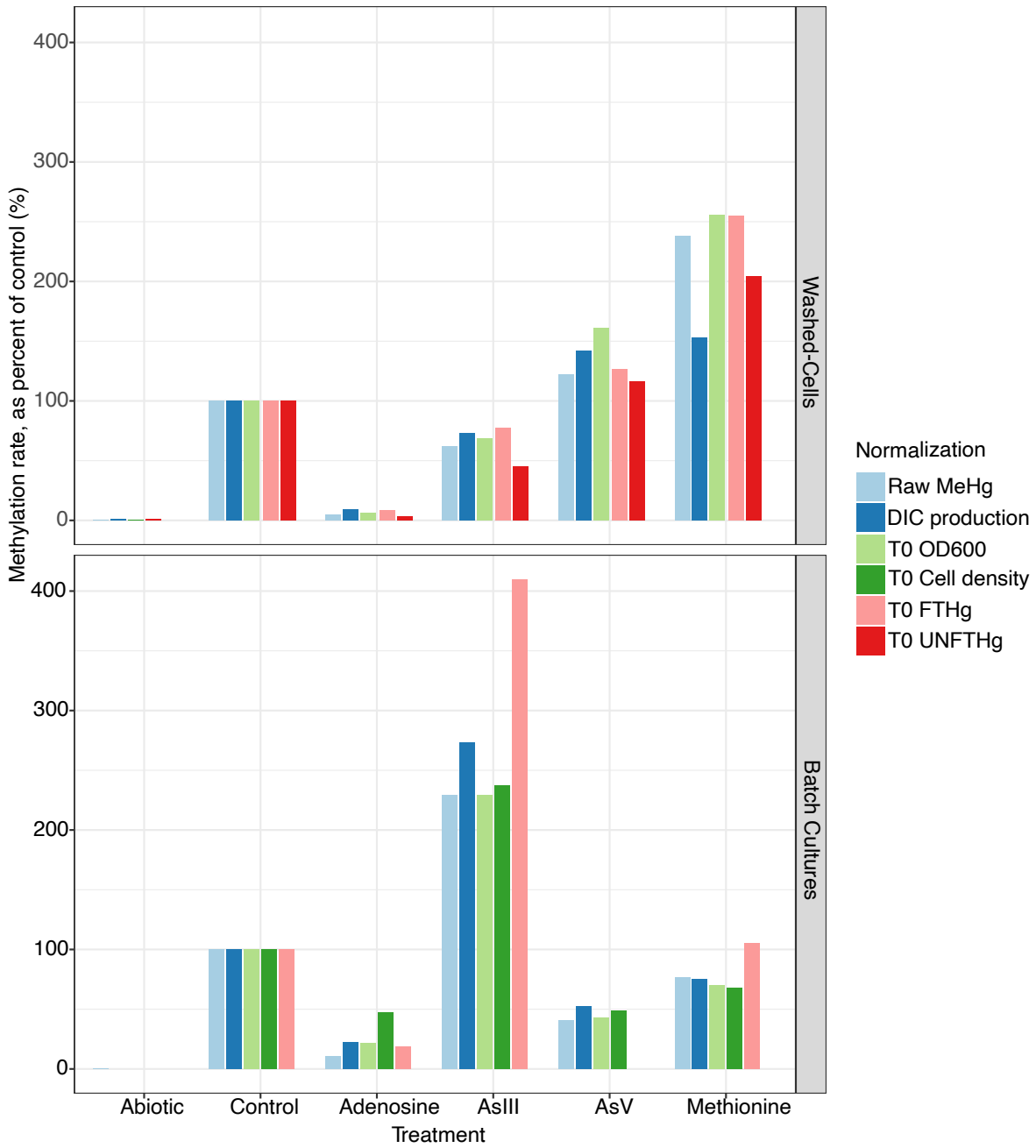

1179

1180 Figure 6. Normalized mercury methylation rates from culture and washed-cell assays. Mercury

1181 methylation rates in *Pseudodesulfovibrio mercurii* ND132 washed-cell (top panel) and batch

1182 culture (bottom panel) assays with test treatments compared to control when normalized to

1183 dissolved inorganic carbon (DIC) production (i.e., CO_2 respiration), optical density (OD_{600}) at

1184 T_0, cell density at T_0, filter-passable total Hg at T_0, and total unfiltered Hg at T_0.

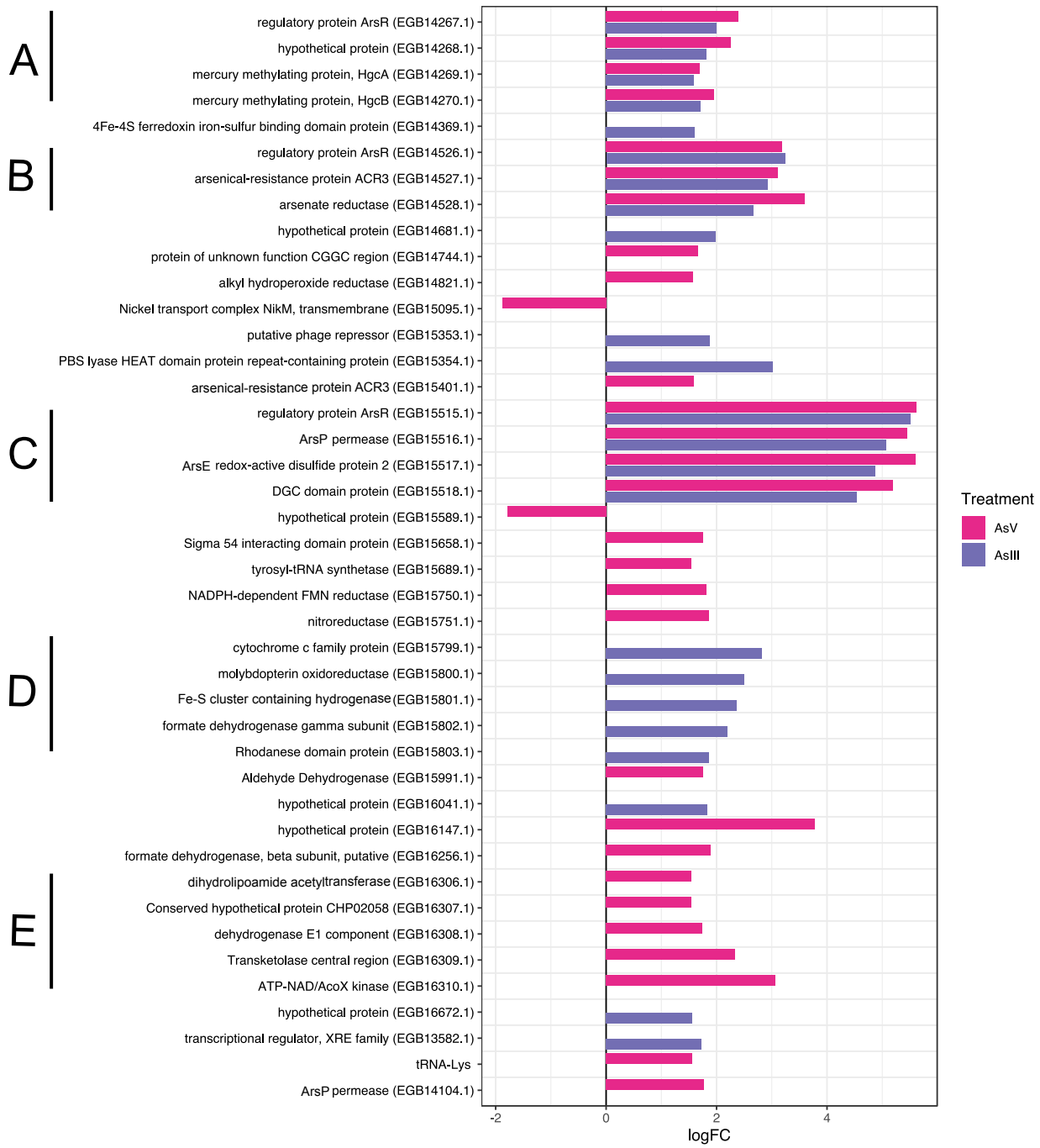

Figure 7. Differential expression of significant features (|log FC| > 1.5, $p < 0.05$) from RNA-seq analyses of As(V) (0.2 mM) and As(III) (0.02 mM) treated washed cells of wild-type *Pseudodesulfovibrio mercurii* ND132. Several putative operons (A-E) had significant differential expression compared to control washed-cells (i.e., no arsenic treatment).

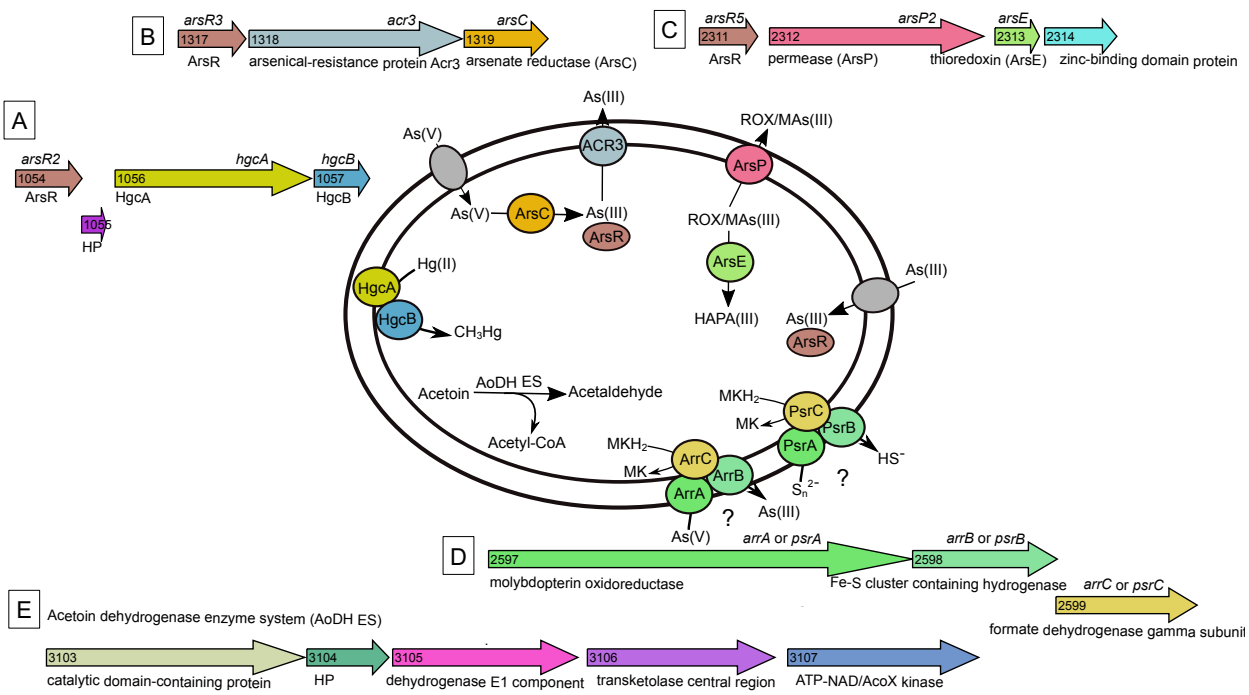

Figure 8. Proposed biochemical reactions for operons that were significantly differentially expressed in *Pseudodesulfovibrio mercurii* ND132 transcriptomes grown with arsenic. This includes genes that are part of the ArsR regulon in ND132, including (A) Hg-methylation genes *hgcA* and *hgcB,* (B) operon that encodes for arsenate reductase (ArsC) and As(III) efflux pump Acr3, and (C) an operon that includes homologues of organoarsenic resistance proteins ArsE and ArsP. Also significantly differentially expressed was an operon (D) that encodes homologues of the polysulfide reductase (Psr) or arsenic respiration complex (Arr), which couples menaquinone (MK) oxidation to periplasmic AsV or sulfur reduction, and (E) a set of genes that encode homologues of the acetoin dehydrogenase enzyme system (AoDH ES). *P. mercurii* ND132 is a confirmed Hg-methylator and can reduce As(V) to As(III). The biochemical mechanism that produces the unknown thioarsenic compound is unknown. To date, *P. mercurii* ND132 has not been tested for organoarsenic resistance or for acetoin degradation. The mechanism for uptake of As(V) and As(III) by ND132 is unknown. Operon graphic made using Gene Graphics(93).